A minimal hepatocyte growth factor mimic acting as a powerful agonist of the MET receptor tyrosine kinase for regeneration of epithelial tissues and organs.

Short Title: Kringle 1 dimer as a minimal MET agonist.

Authors

Bérénice Leclercq[1*], Giovanni de Nola[2*], Alexandra Mougel[1], Solenne Taront[3], Claire Simonneau[4], Federico Forneris[5], Eric Adriaenssens[6], Hervé Drobecq[1], Luisa Iamele[7], Laurent Dubuquoy[3], Ermanno Gherardi[7], Oleg Melnyk[1], Hugo de Jonge[7#], and Jérôme Vicogne[1#].

1. Univ. Lille, CNRS, Inserm, CHU Lille, Institut Pasteur de Lille, U1019 - UMR 9017 - CIIL - Center for Infection and Immunity of Lille, F-59000 Lille, France.

2. Department of Neurobiology, Harvard Medical School, Boston, MA 02115, USA

3. Univ. Lille, Inserm, CHU Lille, U1286 - INFINITE - Institute for Translational Research in Inflammation, F-59000 Lille, France

4. Roche Pharmaceutical Research and Early Development (pRED), Pharmaceutical Sciences, Roche Innovation Center Basel, Basel, Switzerland.

5. The Armenise-Harvard Laboratory of Structural Biology, Dept. Biology and Biotechnology - University of Pavia, via Ferrata 9, 27100 Pavia, Italy

6. Univ. Lille, CNRS, INSERM, CHU Lille, Centre Oscar Lambret, UMR 9020 – UMR 1277 – Canther – Cancer Heterogeneity, Plasticity and Resistance to Therapies, F-59000 Lille, France

7. Department of Molecular Medicine, Pavia University Immunology and General Pathology section, via Ferrata 9, 27100 Pavia (PV), Italy

* contributed equally to this work.

Corresponding authors: e-mail: jerome.vicogne@ibl.cnrs.fr; hugo.dejonge@unipv.it

Abbreviations

ALPHA: amplified luminescent proximity homogenous assay

COPD: chronic obstructive pulmonary disease

HGF/SF: hepatocyte growth factor/scatter factor

Abstract

Degenerative diseases of major internal epithelial organs such as liver, lung, and kidney account for more than one third of mortality worldwide. The huge demand for drugs able to limit epithelial tissue degradation and eventually restore its functionality, place mimics of the hepatocyte growth factor/scatter factor (HGF/SF), the physiological ligand for the MET receptor tyrosine kinase, at the forefront of potential drug candidates. HGF/SF is a growth and motility factor with essential physiological roles in development and regeneration of epithelial organs. Unfortunately, HGF/SF itself is unsuitable for therapy because naturally the factor acts only locally as a pleiotropic factor and has a poor *in vivo* distribution and shelf-life profile. We have therefore designed, produced, solved the crystal structure, and characterized the biochemical and biological properties of K1K1, a new engineered fragment of HGF/SF optimised for applications in tissue/organ regeneration. K1K1, a covalent dimer of the first kringle domain of HGF/SF, is recombinantly produced in bacterial cells, shows superior stability at physiological pH and ionic strength and is a potent receptor agonist as demonstrated in a wide range of biological assays with cells in culture and several *in vivo* studies. K1K1 has broad potential in regenerative medicine with diseases such as acute liver failure, non-alcoholic steatohepatitis, chronic obstructive pulmonary disease, acute kidney injury, and currently lung injury related to respiratory viral infection due to COVID-19.

Key words

HGF/SF, MET receptor agonist, recombinant protein engineering, regenerative medicine.

Significance

The role of HGF/SF and the MET signalling pathway in homeostasis, protection, and regeneration of major organs such as liver, lung, and kidney has been well established. The increasing health burden due to degenerative diseases in our expanding and aging global population has driven research in regenerative therapies and while cell-based therapies have shown promising results, huge costs and technological challenges will hinder widespread application for the foreseeable future. Instead, protein-based therapy, in which a potent MET receptor agonist is administered to patients seems a viable alternative in many diseases currently lacking effective treatment. We describe here the design and characterisation of K1K1, a potent minimal Met receptor agonist with superior properties and equipotent biological activities when compared to native HGF/SF.

Introduction

Life expectancy has more than doubled in less than two hundred years due to a strong reduction of mortality by infectious diseases and malnutrition at young age and a declining mortality at older ages. Astonishingly, in the last five decennia there has been an "epidemic" trend towards younger people reaching old age with increasing levels of disability due to poor diets, smoking and sedentary lifestyles, especially in developed countries (1, 2). The combination of the two trends has caused a dramatic demographic change and an increase in mortality from degenerative diseases (3). Common degenerative diseases of major internal epithelial organs such as alcoholic and non-alcoholic hepatitis (ASH and NASH) leading to chronic liver failure and cancer, chronic obstructive pulmonary disease (COPD) and acute kidney injury (AKI) leading to chronic renal failure affect millions of patients worldwide and are a major causes of mortality (4).

Regardless of initial cause of cell/tissue damage, the response to damage of different epithelial organs display remarkable similarities: loss of parenchymal cells triggers a chronic inflammatory tissue response and the proliferation/activation of non-epithelial cell populations - fibroblasts and myofibroblasts - responsible for the synthesis of extracellular matrix and fibrosis leading to loss of organ function (5). The key to the control of chronic diseases of epithelial organs is protection and regeneration of parenchymal cells in early disease stages prior to the onset of chronic inflammation and fibrosis. This involves therapeutic enhancement of the intrinsic regenerative capabilities of endogenous tissue progenitor or differentiated cells thus preventing the onset of chronic inflammation and fibrosis is promising and may reach large patient populations.

We propose to implement this paradigm by reshaping - through protein engineering - the polypeptide growth/motility factor and potent epithelial morphogen hepatocyte growth factor/scatter factor (HGF/SF) (6, 7) for regenerative medicine. HGF/SF is produced by fibroblasts and other mesenchymal cells that acts in a paracrine manner on target epithelial cells through binding to MET, a receptor tyrosine kinase (8, 9). The evidence for a physiological role of HGF/SF-MET signalling in development and regeneration of liver, lung and kidney is extensive and compelling. HGF/SF-MET is required for lung (10) and kidney (11) development, for survival and regeneration of kidney tubular cells after injury (12) and above all HGF/SF inhibits both lung (13, 14) and kidney (15) fibrosis after injury. These data establish HGF/SF as a key effector of epithelial morphogenesis and a protein with unique therapeutic potential for regeneration of epithelial tissues and organs.

There are several drawbacks, however, in using HGF/SF, the natural MET ligand, for therapy. HGF/SF has a very short half-life (16) and is unstable in physiological buffers (17). Moreover, it has a high affinity for heparan sulphate proteoglycans (HSPG) (18), thereby limiting its tissue/organ penetration and distribution. These properties reflect the nature of HGF/SF as a potent, locally acting chemoattractant, growth factor and morphogen, but constitute appreciable limitations in a therapeutic setting. Here we overcome these limitations by reshaping HGF/SF for therapy through design and synthesis of a novel, ligand-based, minimal MET agonist.

HGF/SF is structurally related to the blood proteinase plasminogen. Its signalling-active two-chain conformation consists of a larger α-chain containing five protein domains, an N-terminal (N) domain homologous to the plasminogen activation peptide and four kringle (K) domains, and a smaller

β-chain containing the C-terminal domain homologous to the catalytic domain of serine proteinases (SPH) (Figure 1A). The evolutionary conserved proteolytic mechanism of activation of the complex blood proteinases and HGF/SF provides a powerful link between the coagulation/fibrinolytic pathways and organ regeneration. Pro-HGF/SF is activated by several of enzymes of the coagulation cascade, as well as by two membrane serine proteinases (matriptase and hepsin) (19). Thus, in embryogenesis, in tissue remodelling, and at sites of tissue damage, activation of the clotting/fibrinolytic pathways causes activation of pro-HGF/SF promoting survival and regeneration of parenchymal cells.

HGF/SF binding to the MET receptor results in dimerization, activation, and subsequent recruitment of scaffolding proteins such as Gab1 and Grb2, which activate Shp2, Ras and ERK/MAPK causing: (i) activation of cell survival pathways through inhibition of caspase-9 and Bad, (ii) changes in gene expression of cell-cycle regulators (such as pRB, Cdk6 and p27), (iii) expression and post-translational activation of matrix metalloproteinases (MMPs) and urokinase (u-PA) leading to alterations of the cytoskeleton necessary for cell migration and division, and (iv) changes in expression of cadherins, Arp2/3, N-WASP, paxillin, integrins and focal adhesion kinase (FAK) essential for cell migration. In this way, HGF/SF-MET signalling causes cell survival, division, migration and a complex morphogenetic programme underlying tissue regeneration (20, 21).

In earlier studies, we defined the structures of an N-terminal fragment of HGF/SF (NK1) that shows good agonist activities and harbours the high-affinity heparin binding site located in the N-domain and the high-affinity binding site for MET (22, 23). Building upon our earlier crystallographic and protein engineering studies (24–31) and recent insights into the role of kringle 1 domain (K1) in agonistic activity (32), we hypothesized that two K1 domains in tandem, forming a covalent K1K1 dimer with reduced heparin affinity, could behave as a minimal receptor agonist endowed with optimal properties for acting *in vivo*. Here we report the design of the K1K1 protein, its expression in bacterial cells and its extensive structural, biochemical, and biological characterization. Furthermore, we have evaluated the protective effect of K1K1 on a validated ASH model. These studies pave the way for more extensive testing of K1K1 *in vivo* in specific models for application in acute and chronic degenerative diseases of liver, lung, and kidney.

Material and Methods

Cloning of K1K1 and K1K1 variants

The cDNA encoding K1K1 and K1K1H6 was generated using a fusion PCR reaction after separate PCR amplification of two K1 domains from a wild-type human NK1 template. The forward primer, ATCATCCCATGGCCATTAGAAACTGCATCATTGGTAAAGGACG, was used to amplify the first kringle domain introducing a 5' NcoI restriction site. The reverse primer for the first K1, TTCAACTTCTGAACACTGAGGA, was used to introduce the linker sequence S E V E placed in-between the two K1 domains. S E V E is naturally found in HGF/SF in between the K1 and K2 domains. The forward primer for the second K1 domain, TCAGAAGTTGAATGCATCATTGGTAAAGGACG, introduces the fusion-overlap with the SEVE linker sequence. A reverse primer with or without a six-histidine tag, ACAGCGGCCGCTCATCAATGATGATGATGATGATGTTCAACTTCTGAACACTGAGGA and ACAGCGGCCGCTCATCATTCAACTTCACTACACTGAGGAAT respectively, introduced two stop codons followed by a NotI restriction site. Following the fusion PCR reaction, the product was digested with NcoI and NotI and ligated into the pET45b(+) expression plasmid (Novagen/EMD Millipore). Integration in the pET45b(+) MCS introduced the additional amino acid sequence M A I R N upstream of the first cysteine of K1 domain.

The heparin mutants S2 and S4 were based on existing kringle-variant NK1 templates. These templates introduced the reverse-charge amino acid substitutions K10E, R12E, K93E, R95E for K1K1S2 and K10E, R12E, K48E, R59E, K93E, R95E, K131E, R142E for K1K1S4.

Protein expression

Recombinant human NK1 protein (residues 28-209) was expressed in *Pichia pastoris* and purified as described in Chirgadze et al., 1999 (26). Recombinant human MET567 was expressed in CHO Lec 3.2.8.1 cells and purified as described in Gherardi et al., 2003 (24). Human HGF/SF was stably expressed in NS0 myeloma cells and purified as described in Gherardi et al., 2006 (34).

For the expression of K1K1 and K1K1 variants, a single colony of freshly transformed *E. coli* BL21(DE3) was used to inoculate an overnight 5 mL Luria broth (LB) culture containing 100 μg/mL of ampicillin. This culture was used to inoculate 500 mL of LB with ampicillin shaking at 250 rpm and grown to an optical density (600 nm) of 0.6-0.8 at 37 °C. The culture was then cooled down to 18 °C while shaking after which IPTG was added to a final concentration of 0.1 mM. The culture was grown at 18 °C with shaking for 24 h after which the bacterial cells were harvested by centrifugation for 30 min at 10,000 rcf at 4 °C and the cell pellet was stored at -80 °C.

K1K1 extraction from inclusion bodies

The frozen bacterial cell pellet was thawed on ice and resuspended in 25 mL 50 mM Tris pH 8.5, 500 mM NaCl, with the addition of one tablet of cOmplete™ EDTA-free Protease Inhibitor Cocktail (Roche), 1 unit of Pierce Universal Nuclease and 10 μg of lysozyme. The suspension was incubated rotating at 4 °C for 30 min before being placed on ice and sonicated using ten pulses of 30 s with 60 s pause in between using a Sonic Ruptor 400 (Omni International) with a OR-T-750 tip at 100% power

output. The suspension was centrifuged at 10,000 rcf for 10 min, the supernatant discarded, and the pellet resuspended in 25 mL 50 mM Tris pH 8.5, 500 mM NaCl with 0.4% Triton X-100 using a glass Potter-Elvehjem tube and PTFE pestle. The suspension was incubated at 4 °C rotating for 30 min after which it was centrifuged at 10,000 rcf for 10 min, the supernatant discarded, and the pellet resuspended in 25 mL 50 mM Tris pH 8.5, 500 mM NaCl with 0.025% NP40 using the Potter-Elvehjem tube and pestle. The suspension was again incubated at 4 °C rotating for 30 min, centrifuged for 10 min at 10,000 rcf, the supernatant discarded, and the pellet resuspended in 25 mL 50 mM Tris pH 8.5, 500 mM NaCl using the Potter-Elvehjem tube and pestle. The suspension was once more incubated at 4 °C rotating for 30 min, centrifuged at 10,000 rcf for 10 min, and the supernatant discarded. The final pellet was resuspended in 20 mL 50 mM Tris pH 8.5, 500 mM NaCl, 2 M arginine, 0.5 mM GSSG, 5 mM GSH. This suspension was incubated for three days at 4 °C on a rotary wheel.

K1K1 purification

After three days of incubation in Tris buffer with arginine, the inclusion body suspension was centrifuged at 20,000 rcf for 30 min at 4 °C. The supernatant was transferred to a new centrifuge tube and centrifuged again at 20,000 rcf for an additional 30 min at 4 °C. Unless a pellet was visible, in which case a third centrifugation was performed in a new tube, the cleared supernatant was diluted 100 times in 2 L of 50 mM Tris pH 7.4, 150 mM NaCl and filtered. The diluted supernatant was loaded onto a 5 mL Heparin HiTrap™ column (GE Healthcare) and eluted with a gradient up to 1 M NaCl, in 50 mM Tris pH 7.4. Peak fractions were pooled, concentrated, and loaded on a HiLoad® 16/600 Superdex 200 pg column (GE Healthcare) equilibrated in 50 mM Tris pH 7.4, 500 mM NaCl. Peak fractions were pooled and concentrated to 5 mg/mL before being used or stored after flash freezing. For K1K1S2 and K1K1S4, instead of Heparin HiTrap™ column, the first step purification was done on a 5 mL HisTrap™ HP column (GE Healthcare).

Protein crystallization and x-ray diffraction

For protein crystallization, K1K1 and K1K1H6 were dialyzed in 10 mM Tris pH 8.5, 100 mM NaCl and concentrated to 12 mg/mL and 11.8 mg/mL respectively. A pre-crystallization screen (PCT, Hampton Research) was performed to confirm these concentrations were favorable for crystallization after which 48-well sitting-drop plates (Hampton Research) were set up using Crystal screen 1 (Hampton Research), JCSG-plus™ (Molecular Dimension) and Morpheus® (Molecular Dimensions) crystallization screens. After overnight incubation at 17 °C, the first crystals appeared in the Morpheus® screen in condition C11 consisting of 100 mM Tris/Bicine pH 8.5, 90 mM sodium nitrate, 90 mM sodium phosphate dibasic, 90 mM ammonium sulphate, 20% v/v glycerol, 10% w/v PEG4000. Further optimization was performed with different protein to crystallization solution ratios (1:2, 1:1, 2:1) in a 24-well plate using hanging drop. After 24 h, good crystals were obtained in a 2:1 protein-to-solution ratio condition. In addition to the cryo-protection intrinsic to the Morpheus® screen, additional glycerol was added up to 25% of the final volume before crystals were collected using a CryoLoop (Hampton Research) and flash frozen and stored in liquid nitrogen. Data was collected at the ESRF in Grenoble, France, at beamline at ID23-1 and was solved by molecular replacement using the NK1 kringle domain

as a search model resulting in a structure with a resolution of 1.6A and an R/Rfree of 20.8/24.3% for K1K1 and a structure with a resolution of 1.8A and an R/Rfree of 18/22% for K1K1H6. Both proteins crystalized in space group P21.

Small Angle X-ray Scattering (SAXS)

Solution scattering data were collected at ESRF BM29 using a sec-1 frame rate on Pilatus 1 M detector located at a fixed distance of 2.87 m from the sample, allowing a global q range of 0.03-4.5 nm with a wavelength of 0.01 nm. SEC-SAXS experiments were carried out using Nexera High Pressure Liquid/Chromatography (HPLC; Shimadzu) system connected online to SAXS sample capillary. For these experiments, 35 µL of each sample at the concentrations indicated in the Table were injected into a Superdex 200 PC 3.2/300 Increase column (GE Healthcare), pre-equilibrated with 25 mM Tris pH 7.4, 150 mM NaCl. Frames corresponding to protein peaks were identified, blank subtracted and averaged using CHROMIXS2. Radii of gyration (Rg), molar mass estimates and distance distribution functions P(r) were computed using the ATSAS package3 in PRIMUS. Modelling of flexible loops and glycosylation were carried out using COOT, CORAL and SASREF. Comparison of experimental SAXS data and 3D models from structural models was performed using CRYSOL. A summary of SAXS data collection and analysis results is shown in Table 1.

Table 1. Summary of SAXS data analysis.

	K1K1	MET567	K1K1+MET567
Data Collection			
BeamLine	ESRF BM29	ESRF BM29	ESRF BM29
Beam energy (keV)	12.5	12.5	12.5
Sample-detector distance (m)	2.867	2.867	2.867
Exposure time (s)	1	1	1
Sample cell thickness (mm)	1	1	1
Sample concentration (mg/mL)	8.5 mg/mL	7.6 mg/mL	12.4 mg/mL
Temperature (°C)	20	20	20
Final q range (nm^{-1})	0.01 - 4	0.01 - 4	0.01 - 4
Data Analysis			
Points used for Guinier analysis	1-94	11-48	2-28
Guinier qR_g limits	1.30	0.97	0.99
Guinier R_g (nm)	2.22	3.23	3.78
I(0) (mm^{-1})	14.8 ± 0.01	64.9 ± 0.04	69.9 ± 0.08
D_{max} (nm)	6.6	11.5	14.2
MW estimation (V_c based) (kDa)	16.5	66.2	83.4

AlphaScreen™ MET binding assay

Saturation assays for binding of K1K1H6 to recombinant MET-Fc protein were performed in 384-well microtiter plates (OptiPlate™-384, PerkinElmer©, CA, USA, 50 µL of final reaction volume). Final concentrations were 0-300 nM for K1K1H6, 0-10 nM for hMET-Fc (8614-MT-100, R&D Systems), 10 µg/mL for Ni-NTA coated donor beads and protein A-conjugated acceptor beads. The buffer used for preparing all protein solutions and the bead suspensions was PBS (10 mM phosphate buffer pH 7.4, 148 mM NaCl, 2mM KCl), 5 mM HEPES pH 7.4, 0.1% BSA. K1K1H6 (10 µL, 0-1.5 µM) was mixed with solutions of MET-Fc (10 µL, 0-50 nM). The mixture was incubated for 10 min (final volume 15 µL). Protein A-conjugated acceptor beads (#6760617C, PerkinElmer©; 10 µL, 50 µg/mL) were then added to the vials. The plate was incubated at 23°C for 30 min in a dark box. Finally, Ni-NTA coated donor beads (6760619C, PerkinElmer©; 10 µL, 50 µg/mL) were added and the plate was further incubated at 23°C for 60 min in a dark box. The emitted signal intensity was measured using standard Alpha settings on an EnSpire® Multimode Plate Reader (PerkinElmer). Measurements are expressed as technical

duplicates (mean+/- SD, n=2). The data corresponding to the 3 nM MET condition was subjected to a non-linear regression analysis using four-parameter sigmoidal equation using Sigmaplot software (version 13).

Cell culture

Madin-Darby Canine Kidney (MDCK, kind gift of Dr Jacqueline Jouanneau, Institut Curie, Paris, France) and Human cervical cancer HeLa cells, purchased from ATCC® (American Type Culture Collection, Rockville, MD, USA), were cultured in DMEM medium (Dulbecco's Modified Eagle's Medium, Gibco, Karlsruhe, Germany), supplemented with 10% FBS (Fetal Bovine Serum, Gibco®, Life technologies, Grand Island, NY, USA) and 1/100 of ZellShield™ (Minerva Biolabs GmbH, Germany). Twenty-four h before treatment, the medium was exchanged with DMEM containing 0.1% FBS, and cells were then treated for subsequent experiments. SKOV-3 cells were cultured in RPMI 1640 medium supplemented with 10% FBS and Penicillin-Streptomycin all purchased from Gibco/ThermoFisher Scientific.

Western Blots

The assay was performed according to Simonneau et al., 2015(32). Hela cells were collected by scraping and lysed on ice with a lysis buffer (20 mM HEPES pH 7.4, 142 mM KCl, 5 mM $MgCl_2$, 1 mM EDTA, 5% glycerol, 1% NP40 and 0.1% SDS) supplemented with freshly added protease inhibitor (1/200 dilution, #P8340, Sigma Aldrich) and phosphatase inhibitor (1/400 dilution, #P5726, Sigma Aldrich). Lysates were clarified by centrifugation (20,000 × g, 15 min) and protein concentration was determined (BCA protein assay Kit, Pierce®, Thermo scientific, IL, USA). The same protein amount (usually 20-30 µg) of cell extracts was separated by NuPAGE gel electrophoresis (4-12% Midi 1.0 mm Bis-Tris precast gels, Life technologies) and electrotransferred to polyvinylidene difluoride (PVDF) membranes (Merck Millipore). Membrane was cut between 80 and 110 kDa marker and at 50 kDa to probe simultaneously phospho or total MET, Akt and ERK. Membranes were probed overnight at 4 °C with primary antibodies diluted to 1/2000 in 5% BSA and 0.1% sodium azide in PBS using specific total MET (#37-0100 Invitrogen), total ERK2 (#SC-154 Tebu-bio), phospho-MET (Y1234/1235, clone CD26, #3077 Cell Signaling), phospho-Akt (S473, clone CD9E, #4060 Cell Signaling), phospho-ERK (T202/Y204, clone E10, #9106 Cell Signaling). After extensive wash with PBS-0.05% Tween® 20 followed incubation with anti-mouse (#115-035-146) or anti-rabbit (#711-035-152) peroxidase-conjugated IgG secondary antibodies (Jackson ImmunoResearch) diluted to 1/30000 in PBS-casein 0.2%. Protein-antibody complexes were visualized by chemiluminescence with the SuperSignal® West Dura Extended Duration Substrate (Thermo scientific) using a LAS-4000 imaging system (GE HeathCare Life Sciences) or X-ray films (CL-XposureTM Film, Thermo scientific).

AlphaScreen™ phosphorylation assay

Measurement of ERK1/2 (T202/Y204) and Akt1/2/3 (S473) activation were performed on HeLa cells using AlphaScreen SureFire Kits (#TGRES500 and #TGRA4S500) according to manufacturer protocol with minor modifications. Into a 96 well plate (#353072, Flacon, Corning), 10 000 HeLa were seeded

in 200 µL of DMEM supplemented with 10% FBS and let attached and grown for 24 h. Cells were next starved in DMEM supplemented with 0.1% FBS for 2 h. Cells were treated for 8 min with MET agonist from 0.3 to 300 pM with HGF/SF, K1K1 or K1K1H6 and from 3 to 3000 pM with K1H6. Cells were quickly washed in cold PBS and AlphaScreen lysis buffer was added for 15 min under middle shaking (600 rpm on orbital rocker, MixMate, Eppendorf). 5 µL of lysate in analyzed by addition of acceptor and donor bead mixes for 2 h at 23 °C. The emitted signal intensity was measured using standard Alpha settings on an EnSpire® Multimode Plate Reader. Measured are expressed has experimental duplicates (mean+/- SD, n=2). The data were subjected to a non-linear regression analysis using four-parameter sigmoidal equation using Sigmaplot software (version 13).

Surface Plasmon Resonance (SPR) analysis

Affinity constants were measured using a Biacore T200 (GE Healthcare) at 25° Celsius using PBST (PBS + 0.05% Tween 20) as running buffer and a flow rate of 30 µl/min. For the measuring of affinity for MET, the receptor fragment MET567 comprising the N-terminal SEMA domain and the cysteine-rich/PSI domain was immobilized at low density (515 RU) using amine-coupling on a CM5 sensor chip (GE Healthcare). A blank inactivated reference channel was used to correct for non-specific binding. 300 seconds injections were done using serial-diluted samples of K1K1, NK1, K1K1S2, and K1K1S4 testing a high range of 2 µM-0.125 µM and low range 0.8 µM-12.5 nM injecting for 300 seconds to reach equilibrium. For the measurement of affinity for heparin, a heparin-coated SC HEP0320.a chip (Xantec) was used. With no reference channel available, all four channels were used for analysis. K1K1, NK1, K1K1S2, and K1K1S4 were injected in a wide range of concentrations (10 µM to 156 nM) for 300 seconds. Biacore Evaluation software version 3.2 was used for calculating affinity constants. Curves were plotted using Graphpad Prism version 5.

SKOV-3 cell migration assays

Agonist-induced cell migration was measured by seeding 50,000 SKOV-3 cells resuspended in serum-free RPMI supplemented with 0.1% BSA (BioFroxx) in each of the upper wells of a 96-well Boyden chamber (AC96, Neuro Probe). HGF/SF, K1K1, K1K1S2, and K1K1S4 was loaded in the lower compartment and cells were left to migrate in a humidified 37°C incubator with 5% CO2 for six hours. Afterwards, non-migrated cells were removed, the cells migrated over the collagen coated (100 µg/mL Purecol, Nutacon) 8 µm pore-size membrane (Neuro Probe) were fixed in 4% paraformaldehyde in PBS and stained using HCS CellMask™ Green stain (ThermoFisher Scientific). Fluorescent intensity was measured using an Azure C600 (Azure Biosystems) and migration was quantified after control-adjustment and charted in Prism (Graphpad).

Madin-Darby canine kidney (MDCK) scatter assay

The assay was performed according to Simonneau et al., 2015 (32) and Stoker et al., 1987 (7). MDCK cells were seeded at low density (2,000 cells/well on a 12-well plate, #353043 Falcon, Corning) in DMEM supplemented with 10% SVF to form compact colonies. After treatment, when colony dispersion was observed and the cells were fixed and colored by Hemacolor® stain (Merck, Darmstadt,

Germany) according to the manufacturer's instructions. Representative images were captured using a phase contrast microscope with 40× and 100× magnification (Nikon Eclipse TS100, Tokyo, Japan).

Morphogenesis Assay

Wells of a black thin clear bottom 24-well plate (#4ti-0241, Brooks Lifesciences) were coated with 200 µL of 2 mg/mL type 1 rat tail collagen (354249, Corning/BD Biosciences) diluted in DMEM equilibrated in 1/10 v/v of 7.5% sodium bicarbonate solution (#25080-060, Gibco, ThermoFisher). Cells (500-700) were seeded into a 500 µL layer of a 1:1 collagen/Growth Factor Reduced Matrigel™ (#354230, Corning/BD Biosciences) mixed in DMEM balance with bicarbonate and were treated twice a week for one month. The cells were then fixed for 24 h with 4% paraformaldehyde in PBS, colored for 3 h with 0.1 mg/L Evans Blue in PBS (#E2129, Sigma Aldrich), extensively wash in PBS and finally nuclei stained with 3 nM DAPI is PBS. Cell were observed using inverted microscope observed and confocal microscope (LSM880 Zeiss) with long distance 10× objective using 488 nm excitation Argon laser and LP 500-750 nm emission filter. 3D reconstitutions (14 µm slices) and maximum intensity projections of z-stack were realized with Zen (v8.1) software.

Survival Assay

In a clear bottom 96-well plate (#353072, Flacon, Corning), 12,500 MDCK cells were seeded and incubated for 24 h in DMEM supplemented with 10% FBS. The culture media was next added with increasing concentrations of the HGF/SF, K1K1, K1K1H6 and NK1 agonists together with the apoptosis inducer anisomycin (1.4 µM) for 15 h. The cells were then washed with PBS to eliminate dead cells and then incubated for 1 h in 200 µL of HBSS (#14025092, Gibco, ThermoFisher) containing 100 µM of Resazurin (#B21187, Sigma Aldrich). Fluorescence was then measured with Envision multimode reader (Ex: 560 nm, Em: 590 nm) with maximal signal gain set (90%) on control cells wells and on top/top reading configuration. The data were normalized to percentage of control cells signal and subjected to a non-linear regression analysis using four-parameter sigmoidal equation with minimum=0 and maximum=100 using Sigmaplot software (version 13).

In vivo MET activation in liver

All experimental procedures were conducted with the approval of the Ethics Committee for Animal Experimentation of the Nord Pas de Calais Region (CEEA 75). For kinetic analysis, 8-week-old FVB mice weighing 19-21 g (Charles River) were intraperitoneally injected with K1K1 (5 µg/mouse) and sacrificed after 10, 30, 60 or 90 min of treatment. For dose-response analysis, 8-week-old FVB mice weighing 19-21 g (Charles River) were intraperitoneally injected with 0.1, 0.5, 1 and 5 µg of K1K1 diluted in 100 µL of PBS and sacrificed per cervical dislocation 10 min after injection. To analyze the effect of the route of administration, 12-week-old C57BL/6 NRJ mice weighing 19-21 g (Janvier Labs) were intraperitoneally or intravenously injected with K1K1 (5 µg/mouse) and sacrificed after 10 min of treatment. Livers were immediately perfused with PBS supplemented with protease and phosphatase inhibitors, collected and then rapidly frozen in liquid nitrogen for subsequent protein extraction and Western blot analysis.

Liver Steatosis Model

Eighty C57BL/6J female mice of 8 to 10 weeks (~19g) provided by Janvier Labs were used in this study. They were housed in temperature- and humidity-controlled rooms, kept on a 12-hours light-dark cycle. Animal procedures were conducted in accordance with French government policies. Mice were fed with a control liquid diet of adapted Lieber DeCarli ad libitum during a 7-day habituation process. Body weight and liquid diet consumption were monitored every two days. Mice were then separated in 6 groups:

- LDC Control Diet-fed mice + vehicle (n=10, Vehicle: 0.0 µg)
- LDC Control Diet-fed mice + product (n=10, highest dose: 10 µg)
- LDC OH-fed mice + vehicle (n=15, Vehicle: 0.0 µg)
- LDC OH-fed mice + product (n=15, Dose 1: 0.4 µg)
- LDC OH -fed mice + product (n=15, Dose 2: 2.0 µg)
- LDC OH -fed mice + product (n=15, Dose 3: 10 µg)

During a 10-days alcoholization period, mice received 5 intraperitoneal injections of 100 µl of sterile PBS or different doses of K1K1 diluted in sterile PBS. Ethanol-fed groups had unlimited access to adapted LDC containing ethanol and control mice were pair-fed with isocaloric control diet over this feeding period. On the 11th day, mice were sacrificed.

Hematoxylin-erythrosin B staining

The livers embedded in paraffin and sectioned at 4µm thick were deparaffinized and rehydrated in successive baths of xylene, absolute ethanol, ethanol 95% and tap water. The slides were stained with hematoxylin (Harris), rinsed, and stained with erythrosine B 0.8% (Sigma). The slides were finally dehydrated and mounted with Eukitt (GmbH). Slides were analysed on a Zeiss Axio Imager M2 microscope. For histological evaluation, a score between 0 and 3 (3 = 75% steatosis) for steatosis was assigned to each section of the liver (3 areas per section).

Real-time quantitative RT-PCR

Livers in 350 µl of RA1 and 3.5µl of β-mercaptoethanol were mixed and frozen at -80°C until RNA extraction. RNA extraction was carried out using the nucleospin RNA kit (Macherey-Nagel). The RNAs were quantified using a Nanodrop and the retro-transcription made using the high-capacity cDNA reverse transcription kit (Thermo Fisher). qPCRs were done by mixing 3.25µl of H2O RNAse free from the RNA extraction kit to 6.25µl of Fast SYBR green Master mix (ThermoFisher) and 0.25µl of reverse and 0.25µl of forward primers diluted in 1/10th in distilled water. qPCRs were performed in a StepOne plus thermocycler (Thermo Fischer). The sequences of the primers used in the study are:

β-actin F: CCA TGT CGT CCC AGT TGG TAA

β-actin R: GAA TGG GTC AGA AGG ACT CCT ATG T

IL-6 F: GTTCTCTGGGAAATCGTGGA

IL-6 R: CAGAATTGCCATTGCACAAC

TNFα F: TGG GAG TAG ACA AGG TAC AAC CC

TNFα R: CAT CTT CTC AAA ATT CGA GTG ACA A

MET F: GACAAGACCACCGAGGATG

MET R: GGAGCCTTCATTGTGAGGAG

ApoB F: TACTTCCACCCACAGTCCC

ApoB R: GGAGCCTAGCAATCTGGAAG

LDLR F: TTCAGTGCCAATCGACTCAC

LDLR R: TCACACCAGTTCACCCCTCT

PPARα F: AGGCAGATGACCTGGAAAGTC

PPARα R: ATGCGTGAACTCCGTAGTGG

Results were presented as levels of expression relative to that of controls after normalizing with β-actin mRNA using the comparative Ct method.

Results

Rational for the design of K1K1. The generation of our recombinant covalent dimer of two HGF/SF kringle 1 domains, designated K1K1, was based on our observation that streptavidin-induced multimerization of a single HGF/SF kringle 1 domain (biotinylated synthetic kringle 1, K1B) resulted in a complex with potent biological activities similar to these of HGF/SF (32). We combined this observation with our understanding of the ligand-receptor interaction, based on extensive structural studies on HGF/SF and NK1 in complex with the MET receptor and the identification of the main, high-affinity receptor binding site in the first kringle domain (26, 33–36).

In our design of recombinant K1K1, we aimed at reproducing the spatial positions of the two kringle 1 domains as observed in the crystal structure of the NK1 dimer (26, 37). Consequently, the resulting covalent kringle 1 dimer no longer dependents on dimerization for its biological activity, as is the case for wild-type NK1 (38, 39), and presents two receptor binding sites on opposite ends. Within the NK1 dimer structure, the distance between the last cysteine in one kringle and the first cysteine in the other kringle is roughly 9 angstroms so we designed a linker to bridge the distance and chose the four amino acid long linker, SEVE, naturally present between kringle 1 and kringle 2 in HGF/SF. This sequence was also introduced at the C-terminus (Figure 1B). A poly-histidine tagged variant, designated K1K1H6, was produced to facilitate certain assays and a single kringle domain with poly-histidine tag (K1H6) was produced as a monovalent control. While the elimination of the N-domain significantly reduced heparin affinity, we also designed two additional variants, K1K1S2 and K1K1S4 (Figure 1A), by introducing reverse-charge mutations in order to diminish residual heparin affinity due to two potential binding sites identified within the K1 domain (40). Both variants carried poly-histidine tags to facilitate purification.

Upon expression in *Escherichia coli*, K1K1 was abundantly present in inclusion bodies and expression at 18°C and induction with a low IPTG concentration (0.1 mM) allowed the production and extraction of fully folded protein from "non-classical" inclusion bodies using a mild arginine-based extraction method based on the work of Jevševar et al. (41) and subsequent work by Singh et al. (42). Expression in these inclusion bodies offers an inexpensive and abundant source of recombinant protein with relatively few contaminants as opposed to soluble bacterial expression. A low-affinity heparin binding site in the kringle domain allowed an effective single-step purification by heparin Sepharose® affinity chromatography following arginine extraction (Figure S1A). After size exclusion chromatography, UPLC-MS analysis confirmed the purity and the congruence between predicted and observed molecular mass for each protein as is shown in Figure S1B and S1C for K1K1 and K1K1H6 respectively. Figure S1D shows all purified recombinant proteins used in this study on Coomassie-stained gel in reducing condition.

Structure determination by x-ray diffraction and SAXS. Purified proteins were used for crystallization experiments using commercial sparse matrix screens and several conditions resulted in the growth of protein crystals at 17°C within days. Crystals were taken for X-ray diffraction experiments using a microfocus beam at the ESRF in Grenoble (France) and resulted in the collection of complete datasets and determination of the molecular structures at 1.6 Å resolution and 1.8 Å for K1K1 and

K1K1H6 respectively. Both proteins crystallized in space group P 1 2_1 1 with K1K1 having two molecules per asymmetric unit and K1K1H6 only one.

Structurally, K1K1 with and without poly-histidine tag are nearly identical, having a backbone root mean square deviation (RMSD) of 0.75 or 1.89 Å (Figure 1C), depending on which of the two molecules in the asymmetric unit of K1K1 is used for alignment with K1K1H6. Both proteins show an elongated "stretched-out" conformation with the MET binding sites exposed at opposite ends and the N- and C-terminus located at the center. In K1K1H6, good electron density was also observed for the poly-histidine tag possibly due to interactions between His172, His173, His175, and His177 with residues Ala4, Asn5, and Thr17 of the N-terminal kringle domain.

Both proteins show a 180-degree rotational symmetry around a central axis presenting both receptor binding sites in nearly identical orientation on either side of the molecule, located around residue Glu37 in the first kringle and residues Glu120 in the second kringle. These residues are equivalent to NK1 residue Glu159 which, among other residues in this region, is involved in the interaction with the SEMA domain of the MET receptor. Presuming the crystal structure presents us with a biologically-relevant conformation, one can envision a binding mode in which two MET receptor monomers are brought in close proximity by binding on opposite sides of K1K1, leading to receptor activation (43). K1K1 therefore presents the most minimalistic peptide-based receptor agonist mimicking the binding and receptor activation mechanism proposed for wild-type NK1 (26) but with the important difference that ligand dimerization is not required. This covalent "mimicry" is more evident when comparing the structures of the NK1 dimer and K1K1. Alignment of the first kringle domain of K1K1 with one of the two kringle domains within the NK1 dimer places the second K1K1 kringle very close to the position of the kringle domain of the other NK1 protomer (Figure 2A). However, the straightened conformation observed in the crystal structure of K1K1, "misaligns" the second K1K1 kringle domain through a rotated of 109.7 degrees resulting in a translation of roughly 14 Å (Figure 2B). With no contacts between the two kringle domains within K1K1 and different conformations of the SEVE linker found in wild-type NK2 as determined by Tolbert and colleagues (22) and in our lab with NK2 in complex with heparin (PDB codes 3HN4 and 3SP8 respectively) (Figure 2C), lead us to believe that the SEVE linker is highly flexible and allows significant conformational freedom. This was confirmed with SAXS measurements which generated an envelope that perfectly accommodates K1K1 volume-wise but only in a more bent conformation (Figure 3A). This is also evident from comparing the experimental scatter curve with one generated based on the crystal structure using CRYSOL. SAXS measurements of MET567 in complex with K1K1 gave a molecular mass estimation of 86.8 kDa and a calculated envelope that corresponds to a 1:1 complex with a "pan handle" extrusion which nicely fits K1K1 bound to the HGF/SF binding site in the SEMA domain (Figure 3B). A model based on the alignment of K1K1 with the crystal structure of NK1 in complex with MET567 obtained in our lab, produced a scatter curve that matched the experimental scatter curve remarkably well (Chi^2=3.6). However, a slightly bent K1K1 conformation matched best with the SAXS envelope. Overall, we have generated compelling structural support for a minimal MET receptor agonist that comprises two covalently linked MET binding sites.

***In vitro* biological data.** The potency of a complex consisting of streptavidin-linked biotinylated synthetic K1 domains in *in vitro* and *in vivo* experiments was previously demonstrated, with MET receptor activation and biological activities similar to those of HGF/SF (32). To analyze MET receptor activation and downstream signaling induced by K1K1, Hela cells were stimulated with recombinant human HGF/SF, K1K1, K1K1H6, and monovalent K1H6 at different concentrations. MET receptor phosphorylation and activation of the key downstream signaling molecules Akt and ERK were confirmed by Western blot (Figure 4A) in which both K1K1 and K1K1H6 stimulate phosphorylation of the pathway down to the lowest tested concentration of 100 pM. As predicted, treatment with K1H6 is indistinguishable from the negative control treatment. We then performed precise quantification of Akt and ERK activation in HeLa cells stimulated with HGF/SF, K1K1, K1K1H6, and K1H6 using ALPHAScreen™ technology. For p-Akt, both K1K1H6 and K1K1 show similar phosphorylation in the low nanomolar range with no significant effect caused by the presence or absence of the poly-histidine tag. Compared to HGF/SF, both variants show lower maximum activation values of Akt (Figure 4B). Interestingly, activation of the Ras-Raf-MAPK pathway as measured by the phosphorylation of ERK showed no significant differences between stimulation by HGF/SF, K1K1H6, or K1K1 at the tested concentrations. Again, no activity was observed with K1H6 even at very high concentrations. We next confirmed the specific binding of K1K1H6 to recombinant human MET-Fc chimera, a soluble dimeric protein comprising the whole extracellular part of the MET receptor (MET922 fused to human IgG1) at different concentrations (Figure 4D, S3A) using the ALPHAScreen™ technology. To accurately determine the KD, we performed full kinetic analysis of K1K1 binding to immobilized MET567 using surface plasmon resonance on a Biacore T200 and measured an apparent KD of 205 nM and a similar KD for NK1 (200 nM, Figure S3B).

Having established MET receptor binding and remarkably potent activation of the MET signaling pathway by both K1K1 and K1K1H6, we subsequently focused on demonstrating its potency in various biological assays. We first performed a cell viability assay based on metabolic activity (resazurin assay, (44)) on MDCK cells incubated overnight (16 hours) in the presence of apoptosis inducer (anisomycin) which prevents protein synthesis and leads to cell death (45). We looked at the cell survival after the addition of HGF/SF, K1K1, K1K1H6 and NK1 at different concentrations during anisomycin treatment. While HGF/SF was most effective, K1K1 and K1K1H6 were equals in preventing cell death and much more potent than native NK1 in this assay (Figure 4E). We also used this assay to validate the specific activities of different preparations of K1K1 and K1K1H6 showing very little batch-to-batch variation and similar relative activity when compared to HGF/SF and NK1 (Figure S4A) confirming the robustness of the expression and purification protocol. An MDCK scatter assay (46) was used as a sensitive assay to determine the minimal concentration needed to activate MET and induce the epithelial-mesenchymal transition disrupting the tight colonies observed when unstimulated. K1K1 was able to exert a scattering effect at a concentration down to 1 pM, ten times lower than native HGF/SF and one thousand times lower than is necessary for NK1 to induce a phenotypic chance in this assay (Figure S4B).

To examine possible effects of specific reverse-charge mutations that altered heparin binding in the kringle domain of NK1 and resulted in the more potent variant 1K1 (28, 47–49), we tested two variants,

K1K1S2 and K1K1S4, and compared them with HGF/SF and K1K1 in an MDCK scattering assay. Both variants had reduced activity with observable scattering for K1K1S2 down to 300 pM and no scattering observed at 100 pM while K1K1 still showed activity at a concentration ten times lower (10 pM). K1K1S4 only showed activity in the low nanomolar range and was inactive at 1 nM (Figure 5A). To confirm these results, we performed a 3D morphogenesis assay using the same MDCK cells (Figure 5B and Figure S5A and B) and confirmed the results obtained with the scatter assay indicating that the reverse-charge mutations reduced the biological activity of K1K1S2 and K1K1S4. This loss of biological activity was also quantitatively confirmed in SKOV3 cells using a Boyden chamber migration assay (Figure 5C). Finally, we confirmed this loss of biological activity at the level of the MET receptor signaling pathway by investigating the phosphorylation status of MET, Akt, and ERK. In agreement with observed biological activities, K1K1S2 and K1K1S4 are weaker agonists than K1K1 by one and two orders of magnitude respectively (Figure S5C) suggesting that the heparin binding site within the K1 domain plays a role in the MET activation.

***In vivo* activation of MET signaling.** With the *in vitro* assays clearly demonstrating the superior potency of K1K1 over NK1 and in several assays, matching or even surpassing native HGF/SF, we were keen to start several *in vivo* mouse studies to look at the effects of K1K1. We first confirmed that the injection route, intraperitoneal (I.P.) versus intravenous (I.V.), did not affect the biological availability and activity in the mouse liver by measuring phosphorylation of the MET receptor, Akt, and ERK by Western blot on liver homogenates 10 minutes after injection (Figure S6). Since no significant difference between the administration routes was observed, for convenience all subsequent injections were done by I.P. To study the effect of different dosage, 8-week-old FVB mice were injected with different amounts of K1K1 (0.1 to 5 µg) after which the animal was sacrificed 10 minutes later and the phosphorylation status of the MET signaling pathway was established in the liver homogenates. Control as well as 0.1 µg of K1K1 did not result in any detectable MET, Akt, and ERK phosphorylation signal while injection of 0.5, 1, and 5 µg gave uniform activation of the pathway (Figure 6A). A second experiment in which 5 µg of K1K1 was injected was performed to determine the duration of the stimulation by sacrificing the animals at 10, 30, 60, and 90 minutes, showing a diminishing signal over time detectable up to 60 min (Figure 6B).

***In vivo* efficacy of K1K1 in the treatment of alcoholic steatohepatitis.** To evaluate the *in vivo* efficacy of K1K1 in liver diseases, we have used a validated mouse model of subchronic alcohol exposure, the adapted Lieber DeCarli (LDC) model (50) in order to study steatosis, a common feature of several liver diseases.

As expected, alcohol consumption induced steatosis in liver of mice fed with alcohol (LDC + Vehicle group) which was not observed in mice fed with a control diet (Control + Vehicle) or a control diet with K1K1 treatment (Control + 10µg K1K1) (Figure 7A and Figure S7A). The treatment with different doses of K1K1 (0.4, 2 and 10 µg) significantly decreases the steatosis in mice fed with alcohol (LDC + K1K1) (Figure 7B). We then determine important factors involved in steatosis improvement. K1K1 treatment was able to significantly increase mRNA expression of ApoB, PPARα and LDLR (Figure 7B). Alcohol consumption also resulted in a moderate increase in the liver expression of the

proinflammatory cytokines TNFα and IL-6 (Figure S7B). In LDC mice, the highest doses of K1K1 (2 and 10µg) significantly decreased the mRNA expression of TNFα and IL-6. Interestingly, while mRNA expression of MET decreased by ethanol exposure alone, it was induced by K1K1 treatment (Figure S7B).

Taken together these results demonstrated that K1K1 significantly improved steatosis in a mouse model of liver injury. This therapeutic effect is believed to be mediated in part by the increase of protective factors such as ApoB and PPARα and the lowering of proinflammatory cytokines, induced by K1K1 treatment.

Discussion

The protection and regeneration of liver by treatment with HGF/SF has been of particular interest which is not surprising as it was discovered as a growth factor dramatically increased in serum after partial hepatectomy (51) and at the same time was identified as a scatter factor (SF). Indeed, HGF/SF has been extensively tested in *in vivo* mouse and rat liver damage models (52) and is tested in clinical trials including one for Fulminant Hepatic Failure (NCT00225901). The studies involved different delivery formats and delivery routes of the native growth factor, such as injection of recombinant HGF/SF (53), HGF/SF gene delivery (54), and more recently HGF/SF-transfected mesenchymal stem cells (55). While all these studies provide clear evidence for the therapeutic potential of HGF/SF and many similar studies exist on diseases of kidney, lung, heart, and the vascular and nervous system, they have also highlighted significant limitations in the (cost) effective delivery of the protein at the site of damage. There is therefore an urgent need for alternative agonistic molecules and more effective delivery methods.

Several MET agonists have been developed over the years, most notably Magic-F1 (56) , eNK1 (57), agonistic monoclonal antibodies (58, 59), a group of synthetic cyclic peptides (60) and recently an aptamer (61). Most relevant to our study are Magic-F1 and eNK1 as they are both based on dimers of HGF/SF domains. Magic-F1 comprises a tandem repeat of the HGF/SF N-domain and the first two kringle domains and showed noticeable anti-apoptotic and pro-differentiation activity and promoted muscle regeneration in a mouse model. However, its administration relied on injection and electrotransfer of the gene directly into the muscle tissue of the mouse or alternatively needed adenovirus-mediated gene delivery which might hamper wide-spread therapeutic application. eNK1, a disulphide-linked dimer of a more stable variant of NK1 also shows good agonistic activity superior to native NK1. However, Magic-F1 and dimeric eNK1 both contain two copies of the high-affinity heparin binding site in the N-domain creating the same problem that native HGF/SF has: limited diffusion and tissue penetration. This was well demonstrated in our earlier studies on semi-synthetic kringle 1 (K1B/S) whereby intravenous injection of HGF/SF could only protect liver from Fas-induced fulminant hepatitis at very high doses while the kringle still showed protective activity at very low doses (32). For this reason, reduced affinity for heparin was one of the K1K1 design objectives. SPR analysis of heparin

affinity confirmed a strong ten-fold reduction of heparin binding in K1K1 (KD ~5.6 μM) and negligible affinity in K1K1S2 and K1K1S4, compared to NK1 (KD ~0.43 μM) (Figure S8). Further evidence for the improved diffusion characteristics of K1K1 come from the lack of a noticeable difference between intravenous and intraperitoneal administration (Figure S6). Interestingly, further reduction of heparin affinity through reverse-charge mutagenesis in K1K1S2 and K1K1S4 resulted in a loss of potency in all assays (Figure 5A-C and Figure S5A-C). While K1K1 showed biological active equipotent to HGF/SF, demonstrating that high affinity for heparin or heparan sulphate associated with the N domain is not a prerequisite for receptor activation, the loss of activity observed with the two mutant variants is not easily explained without further biochemical and structural investigation. It might be that heparin/heparan plays a role in orienting and/or rigidifying the overall structure of K1K1 or affects the local conformation of the individual kringle domains in K1K1.

All things considered, we believe that with our design of K1K1 we generated the smallest possible MET receptor agonist based on a native sequence, displaying superior potency and optimal diffusibility and stability. These structural, biochemical, and biological data are in full agreement to use K1K1 as a diffusible MET agonist in many pathologies where the HGF/SF-MET signalling is defective or insufficient. Liver is thus an appropriate model to evaluate K1K1 as a potential therapeutic. In particular, evidence has been accumulated to show that the "HGF/SF approach" is a good candidate to treat liver fibrosis, cirrhosis or alcoholic steatohepatitis (62–65). Matsuda and colleagues have demonstrated that HGF/SF administration promotes rat liver cells recovery from alcohol-induced fatty liver (66). This was confirmed by a recent study showing that MET gene deletion in mice hepatocytes, led to hyperlipidemia and severe steatosis as well as abnormal β-oxidation of free fatty acids (67). This hepatocyte invalidation results in an earlier initiation of hepatic steatosis and deposition of collagen indicating faster progression to hepatic fibrosis. All these data clearly show that HGF/SF is an essential actor for morphogenesis, and fibrosis/cirrhosis protection providing a unique therapeutic potential for the regeneration and the protection of the liver. Using mouse models mimicking ASH, we demonstrated that a regular K1K1 injection decreases inflammation and steatosis.

Altogether, the results obtain in this work highlights the therapeutic potential of K1K1. The ease of production and attained purity are further attributes making this molecule an attractive therapeutic candidate for the treatment of both acute and chronic diseases of major epithelial organs with possible additional therapeutic applications in neurodegenerative diseases such as amyotrophic lateral sclerosis, multiple sclerosis, and spinal cord injuries, based on several promising studies done with HGF/SF (68–71).

Material and Methods

See STAR Methods section.

Acknowledgments

We thank SATT-Nord (France) for financing the proof-of-concept experiments, Thierry Chassat from the PLETHA animal Facility in Lille Pasteur Institute for helpful advises and kind availability.

The production, purification, and characterisation of K1K1 in Pavia was made possible through the "Dipartimento di Eccellenza" funding scheme (Italian Ministry of Education). We would like to acknowledge Dr Dimitri Y. Chirgadze at the department of Biochemistry, University of Cambridge (UK) for his help in solving the structure of K1K1 and K1K1H6 and are grateful for his support and contributions to our work over the many years we collaborated. We would also like to thank Maria Cristina Barbieri for her continued technical support in Pavia.

Figure Legends

Figure 1. Domain architecture of MET agonists and crystal structure of K1K1 and K1K1H6.
(A) Schematic representation of HGF/SF, NK1, K1K1, K1K1 variants, full length MET and the MET567 fragment. Individual domains (boxes) with positions of domain boundaries indicated above. CR: cysteine rich, Ig: immunoglobulin like, SPH: serine protease homology, S-S: disulphide bonds, TK: tyrosine kinase, TM: transmembrane domain. (B) Amino acid sequence of K1K1H6 with SEVE linker and poly-histidine tag in grey boxes. (C) The crystal structure of the two molecules of K1K1 (turquoise and cyan) and K1K1H6 (green) showing the straight conformation and the N-terminus ("N") and C-terminus ("C") located centrally in the linker region. Alignment of both all single K1K1 molecules found in the asymmetric units, K1K1 A, K1K1 B and K1K1H6 shows a nearly identical overall structure with an RMSD ranging from 0.745 to 1.89 Å. The C-terminal poly-histidine tag of K1K1H6 is making contacts with residues in the N-terminal kringle domain. A HEPES molecule is present in each "lysine-binding" pocket of K1K1H6.

Figure 2. Structural alignment of K1K1 with NKI dimer.
(A) Two 90° views of the K1K1-NK1 alignment using one kringle of K1K1 (green) with the kringle of one protomer (magenta) in the NK1 dimer. The alignment projects the second K1K1 kringle across and positions it close to but not in the same position as the second kringle domain in the NK1 dimer (cyan). (B) The straight, stretched out conformation of K1K1 misaligns the second kringle domain by a rotation of 109.7° leading to a translation of 13.4 Å. (C) The linker based on the naturally occurring linker sequence between kringle 1 and kringle 2 in HGF/SF, SEVE, is straight in K1K1 (green) and has a different conformation in two NK2 structures available (3HN4 in magenta and 3SP8 in cyan obtained in our lab). Numbering is given in italic from the last cysteine of kringle 1 (C206 in NK2) until the first cysteine in kringle 2 (C211 in NK2) with equivalent K1K1 residues in bold.

Figure 3. SAXS models for K1K1 alone and in complex with MET567.
(A) The measured SAXS envelope is not compatible with the elongated K1K1 crystal structure (pink) but perfectly accommodates a bend conformation of K1K1 (cyan). To fit the SAXS envelope, the linker region is bent by roughly 60° (B) The *ab initio* SAXS envelope of the 1:1 complex of K1K1 and MET567 shows a "pan-handle" extension, which accommodates K1K1. The CR domain is partially protruding from the bottom of the envelope and extra volume might be occupied by glycosylated side chains.

Figure 4. *In vitro* activity of the HGF/SF, K1K1, K1K1H6, and K1H6.
(A) Phosphorylation analysis by Western blot on Hela cell lysates after stimulation with ligands for 10 min at concentrations indicated above each lane. Loading controls are based on total MET, total Akt, and total ERK present in each lane. (B) AlphaScreen™ measurements of p-Akt and (C) p-ERK activation in HeLa cells after 10 min stimulation with K1K1, K1K1H6, HGF/SF and K1H6. (D) Binding determination using the ALPHAScreen™ saturation binding assay. Seven concentrations of K1K1H6 were tested on several different concentrations of MET-Fc (AA 25-922) (Suppl. Fig S3A). Shown is the binding of K1K1H6 to 3 nM MET-Fc. (E) Ligand induced MDCK survival after overnight treatment with the apoptotic inducer anisomycin. Indicated is the percentage of viable cells compared to no-anisomycin treatment after exposure to HGF/SF, K1K1, K1K1H6, and NK1 at different concentrations.

Figure 5. Effects on cell motility, migration, and morphology.
(A) MDCK cell scattering at different concentrations K1K1, K1K1S2 and K1K1S4 showing the lowest concentration at which each protein is still active and the subsequent dilution at which no more scattering is observed. HGF/SF is used as positive control to generate maximum scattering. For complete half-log dilution of agonist series, see Data Source Image File. (B) 3D reconstruction by z-stacking of fluorescence microscopy images taken of large MDCK cell colonies stimulated with 100 pM HGF/SF or 10 nM K1K1 and mutants for four weeks. The combined fluorescence of DAPI (red) and Evans blue staining (grey scale) shows the extensive morphological change and tubulogenesis induced by both proteins. (C) Boyden chamber migration assay using SKOV3 cells. Cells were treated for 6 hours with indicated concentrations of HGF/SF, K1K1, K1K1S2 and K1K1S4 after which the migrated cells were detected with CellMask™ Green stain. Migration is presented as fold increase over control. Error bars represent mean +/- SD based on quadruplicates (n=4).

Figure 6. Dose response and MET pathway activation kinetics after intraperitoneal injection.
(A) 8-week-old FVB mice were injected with PBS (Ctrl) or different amounts of K1K1 after which MET, AKT, and ERK phosphorylation in liver homogenate was determined using Western blot. Mice were sacrificed 10 minutes after injection. Results are presented as experimental duplicate (n=2). (B) MET, AKT, and ERK phosphorylation were detected by Western blot at different time points after injection of 5 µg of K1K1. Results are presented as experimental duplicate (n=2) except for control and 10 min conditions. Both blots present total MET, Akt and ERK proteins as loading controls.

Figure 7. *In vivo* evaluation of the efficacy of the K1 dimer in a mouse model of alcoholic steatohepatitis.
(A) Hematoxylin-erythrosin B staining of mouse livers submitted to an adapted Lieber DeCarli model (x20). Analyses were performed on 10 animals in control groups (Ctr + Vehicle and Ctr +10 µg K1K1) and 15 animals in ethanol treated groups (LDC ± K1K1). Scale bar = 50 µm (B) Steatosis was quantified in each mouse liver using a

steatosis score (see material and methods). Results are expressed as mean ± SD (C) The mRNA expression of triglyceride metabolism markers (ApoB, PPARa, and LDLR) was analysed in mouse livers using RT-qPCR with b-actin as housekeeping gene. Results are expressed in relative units (RU) and represented as mean ± SD.

References

1. H. Beltra, Beltrán-Sánchez H, Soneji S, Crimmins EM. Past, Present, and Future of Healthy Life Expectancy. Cold Spring Harb Perspect Med. 2015;5(11):a025957. Published 2015 Nov 2. doi:10.1101/cshperspect.a025957. *Cold Spring Harb Perspect Med.* **19**, 468 (2016).
2. B. M. Popkin, Li. S. Adair, S. W. Ng, Global nutrition transition and the pandemic of obesity in developing countries. *Nutr. Rev.* **70**, 3–21 (2012).
3. M. Naghavi, *et al.*, Global, regional, and national age-sex specific mortality for 264 causes of death, 1980–2016: a systematic analysis for the Global Burden of Disease Study 2016. *Lancet* **390**, 1151–1210 (2017).
4. R. Lozano, *et al.*, Global and regional mortality from 235 causes of death for 20 age groups in 1990 and 2010: a systematic analysis for the Global Burden of Disease Study 2010. *Lancet* **380**, 2095–2128 (2012).
5. A. Ahmad, R. Ahmad, Understanding the mechanism of hepatic fibrosis and potential therapeutic approaches. *Saudi J. Gastroenterol.* **18**, 155–67 (2012).
6. T. Nakamura, K. Nawa, A. Ichihara, N. Kaise, T. Nishino, Purification and subunit structure of hepatocyte growth factor from rat platelets. *FEBS Lett.* **224**, 311–316 (1987).
7. M. Stoker, E. Gherardi, M. Perryman, J. Gray, Scatter factor is a fibroblast-derived modulator of epithelial cell mobility. *Nature* **327**, 239–42 (1987).
8. M. Park, M. Dean, K. Kaul, M. J. Braun, M. A. Gonda, G. Vande Woude, Sequence of MET protooncogene cDNA has features characteristic of the tyrosine kinase family of growth-factor receptors. *Proc. Natl. Acad. Sci. U. S. A.* **84**, 6379–6383 (1987).
9. D. P. Bottaro, J. S. Rubin, D. L. Faletto, A. M. Chan, T. E. Kmiecik, G. F. Vande Woude, S. A. Aaronson, Identification of the hepatocyte growth factor receptor as the c-met proto-oncogene product. *Science* **251**, 802–804 (1991).
10. S. Padela, J. Cabacungan, S. Shek, R. Belcastro, M. Yi, R. P. Jankov, A. K. Tanswell, Hepatocyte Growth Factor Is Required for Alveologenesis in the Neonatal Rat. *Am. J. Respir. Crit. Care Med.* **172**, 907–914 (2005).
11. D. Zhou, R. J. Tan, L. Lin, L. Zhou, Y. Liu, Activation of hepatocyte growth factor receptor, c-met, in renal tubules is required for renoprotection after acute kidney injury. **84**, 509–520 (2013).
12. Y. Zhou, W. Dai, C. Lin, F. Wang, L. He, M. Shen, P. Chen, C. Wang, J. Lu, L. Xu, X. Xu, C. Guo, Protective Effects of Necrostatin-1 against Concanavalin A-Induced Acute Hepatic Injury in Mice. *Mediators Inflamm.* **2013**, 1–15 (2013).
13. M. Dohi, T. Hasegawa, K. Yamamoto, B. C. Marshall, Hepatocyte Growth Factor Attenuates Collagen Accumulation in a Murine Model of Pulmonary Fibrosis. **162**, 2302–2307 (2000).
14. S. Mizuno, K. Matsumoto, M.-Y. Li, T. Nakamura, HGF reduces advancing lung fibrosis in mice: a potential role for MMP-dependent myofibroblast apoptosis. *FASEB J.* **19**, 580–2 (2005).
15. Y. Liu, Hepatocyte growth factor in kidney fibrosis: therapeutic potential and mechanisms of action. *Am. J. Physiol. Physiol.* **287**, F7–F16 (2004).
16. F. Roos, A. M. Ryan, S. M. Chamow, G. L. Bennett, R. H. Schwall, Induction of liver growth in normal mice by infusion of hepatocyte growth factor/scatter factor. *Am. J. Physiol.* **268**, G380-6 (1995).
17. J. Ross, E. Gherardi, N. Mallorqui-Fernandez, M. Bocci, A. Sobkowicz, M. Rees, A. Rowe, S. Ellmerich, I. Massie, J. Soeda, C. Selden, H. Hodgson, Protein engineered variants of hepatocyte growth factor/scatter factor promote proliferation of primary human hepatocytes and in rodent liver. *Gastroenterology* **142**, 897–906 (2012).

18. G. Hartmann, T. Prospero, V. Brinkmann, Ö. Ozcelik, G. Winter, J. Hepple, S. Batley, F. Bladt, M. Sachs, C. Birchmeier, W. Birchmeier, E. Gherardi, Engineered mutants of HGF/SF with reduced binding to heparan sulphate proteoglycans, decreased clearance and enhanced activity in vivo. *Curr. Biol.* **8**, 125–135 (1998).

19. K. A. Owen, D. Qiu, J. Alves, A. M. Schumacher, L. M. Kilpatrick, J. Li, J. L. Harris, V. Ellis, Pericellular activation of hepatocyte growth factor by the transmembrane serine proteases matriptase and hepsin, but not by the membrane-associated protease uPA. *Biochem. J.* **426**, 219–28 (2010).

20. C. Birchmeier, W. Birchmeier, E. Gherardi, G. F. Vande Woude, Met, metastasis, motility and more. *Nat. Rev. Mol. Cell Biol.* **4**, 915–25 (2003).

21. E. Gherardi, W. Birchmeier, C. Birchmeier, G. Vande Woude, Targeting MET in cancer: rationale and progress. *Nat. Rev. Cancer* **12**, 89–103 (2012).

22. W. D. Tolbert, J. Daugherty-Holtrop, E. Gherardi, G. Vande Woude, H. E. Xu, Structural basis for agonism and antagonism of hepatocyte growth factor. *Proc. Natl. Acad. Sci. U. S. A.* **107**, 13264–9 (2010).

23. O. Holmes, S. Pillozzi, J. a Deakin, F. Carafoli, L. Kemp, P. J. G. Butler, M. Lyon, E. Gherardi, Insights into the structure/function of hepatocyte growth factor/scatter factor from studies with individual domains. *J. Mol. Biol.* **367**, 395–408 (2007).

24. E. Gherardi, M. Youles, R. Miguel, T. Blundell, L. Iamele, J. Gough, A. Bandyopadhyay, G. Hartmann, P. Butler, Functional map and domain structure of MET, the product of the c-met protooncogene and receptor for hepatocyte growth factor/scatter factor. *Proc. Natl. Acad. Sci. U. S. A.* **100**, 12039–12044 (2003).

25. H. H. Niemann, V. Jäger, P. J. G. Butler, J. van den Heuvel, S. Schmidt, D. Ferraris, E. Gherardi, D. W. Heinz, Structure of the human receptor tyrosine kinase met in complex with the Listeria invasion protein InlB. *Cell* **130**, 235–46 (2007).

26. D. Y. Chirgadze, J. P. Hepple, H. Zhou, R. a Byrd, T. L. Blundell, E. Gherardi, Crystal structure of the NK1 fragment of HGF/SF suggests a novel mode for growth factor dimerization and receptor binding. *Nat. Struct. Biol.* **6**, 72–9 (1999).

27. E. Gherardi, S. Sandin, M. V Petoukhov, J. Finch, M. E. Youles, L.-G. Ofverstedt, R. N. Miguel, T. L. Blundell, G. F. Vande Woude, U. Skoglund, D. I. Svergun, Structural basis of hepatocyte growth factor/scatter factor and MET signalling. *Proc. Natl. Acad. Sci. U. S. A.* **103**, 10–11 (2006).

28. D. Lietha, D. Y. Chirgadze, B. Mulloy, T. L. Blundell, E. Gherardi, Crystal structures of NK1-heparin complexes reveal the basis for NK1 activity and enable engineering of potent agonists of the MET receptor. *EMBO J.* **20**, 5543–5555 (2001).

29. W. D. Tolbert, J. Daugherty, C. Gao, Q. Xie, C. Miranti, E. Gherardi, G. Vande Woude, H. E. Xu, A mechanistic basis for converting a receptor tyrosine kinase agonist to an antagonist. *Proc. Natl. Acad. Sci. U. S. A.* **104**, 14592–7 (2007).

30. W. Tolbert, J. Daugherty-Holtrop, E. Gherardi, G. Vande Woude, H. Xu, Structural basis for agonism and antagonism of hepatocyte growth factor. *Proc. Natl. Acad. Sci. U. S. A.* **107**, 13264–9 (2010).

31. M. Youles, O. Holmes, M. V Petoukhov, M. a Nessen, S. Stivala, D. I. Svergun, E. Gherardi, Engineering the NK1 fragment of hepatocyte growth factor/scatter factor as a MET receptor antagonist. *J. Mol. Biol.* **377**, 616–22 (2008).

32. C. Simonneau, B. L. Bérénice Leclercq, A. Mougel, E. Adriaenssens, C. Paquet, L. Raibaut, N. Ollivier, H. Drobecq, J. Marcoux, S. Cianférani, D. Tulasne, H. de Jonge, O. Melnyk, J. Vicogne, Semi-synthesis of a HGF/SF kringle one (K1) domain scaffold generates a potent in vivo MET receptor agonist. *Chem. Sci.* **6**, 2110–2121 (2015).

33. M. Blaszczyk, N. J. Harmer, D. Y. Chirgadze, D. B. Ascher, T. L. Blundell, Achieving high signal-to-noise in cell regulatory systems: Spatial organization of multiprotein transmembrane assemblies of FGFR and MET receptors. *Prog. Biophys. Mol. Biol.* **118**, 103–111 (2015).
34. E. Gherardi, S. Sandin, M. V Petoukhov, J. Finch, M. E. Youles, L.-G. Ofverstedt, R. N. Miguel, T. L. Blundell, G. F. Vande Woude, U. Skoglund, D. I. Svergun, Structural basis of hepatocyte growth factor/scatter factor and MET signalling. *Proc. Natl. Acad. Sci. U. S. A.* **103**, 4046–51 (2006).
35. L. E. Donate, E. Gherardi, N. Srinivasan, R. Sowdhamini, S. Aparicio, T. L. Blundell, Molecular evolution and domain structure of plasminogen-related growth factors (HGF/SF and HGF1/MSP). *Protein Sci.* **3**, 2378–94 (1994).
36. N. A. Lokker, L. G. Presta, P. J. Godowski, Mutational analysis and molecular modeling of the N-terminal kringle-containing domain of hepatocyte growth factor identifies amino acid side chains important for interaction with the c-Met receptor. *Protein Eng.* **7**, 895–903 (1994).
37. M. Ultsch, N. a Lokker, P. J. Godowski, A. M. de Vos, Crystal structure of the NK1 fragment of human hepatocyte growth factor at 2.0 å resolution. *Structure* **6**, 1383–1393 (1998).
38. R. H. Schwall, L. Y. Chang, P. J. Godowski, D. W. Kahn, K. J. Hillan, K. D. Bauer, T. F. Zioncheck, Heparin induces dimerization and confers proliferative activity onto the hepatocyte growth factor antagonists NK1 and NK2. *J. Cell Biol.* **133**, 709–18 (1996).
39. H. Sakata, S. J. Stahl, W. G. Taylor, J. M. Rosenberg, K. Sakaguchi, P. T. Wingfield, J. S. Rubin, Heparin binding and oligomerization of hepatocyte growth factor/scatter factor isoforms. Heparan sulfate glycosaminoglycan requirement for Met binding and signaling. *J. Biol. Chem.* **272**, 9457–9463 (1997).
40. D. Lietha, D. Y. Chirgadze, B. Mulloy, T. L. Blundell, E. Gherardi, Crystal structures of NK1-heparin complexes reveal the basis for NK1 activity and enable engineering of potent agonists of the MET receptor. *EMBO J.* **20**, 5543–55 (2001).
41. S. Jevševar, V. Gaberc-Porekar, I. Fonda, B. Podobnik, J. Grdadolnik, V. Menart, Production of nonclassical inclusion bodies from which correctly folded protein can be extracted. *Biotechnol. Prog.* **21**, 632–639 (2005).
42. A. Singh, V. Upadhyay, A. K. Upadhyay, S. M. Singh, A. K. Panda, Protein recovery from inclusion bodies of Escherichia coli using mild solubilization process. *Microb. Cell Fact.* **14** (2015).
43. M. A. Lemmon, J. Schlessinger, Cell signaling by receptor tyrosine kinases. *Cell* **141**, 1117–34 (2010).
44. J. O'Brien, I. Wilson, T. Orton, F. Pognan, Investigation of the Alamar Blue (resazurin) fluorescent dye for the assessment of mammalian cell cytotoxicity. *Eur. J. Biochem.* **267**, 5421–5426 (2000).
45. T. Mosmann, Rapid colorimetric assay for cellular growth and survival: application to proliferation and cytotoxicity assays. *J. Immunol. Methods* **65**, 55–63 (1983).
46. M. Stoker, M. Perryman, An epithelial scatter factor released by embryo fibroblasts. *J. Cell Sci.* **77**, 209–23 (1985).
47. J. Ross, E. Gherardi, N. Mallorquifernandez, M. Bocci, A. Sobkowicz, M. Rees, A. Rowe, S. Ellmerich, I. Massie, J. Soeda, C. Selden, H. Hodgson, Protein engineered variants of hepatocyte growth factor/scatter factor promote proliferation of primary human hepatocytes and in rodent liver. *Gastroenterology* **142**, 897–906 (2012).
48. R. Sinha Roy, S. Soni, R. Harfouche, P. R. Vasudevan, O. Holmes, H. de Jonge, A. Rowe, A. Paraskar, D. M. Hentschel, D. Chirgadze, T. L. Blundell, E. Gherardi, R. A. Mashelkar, S. Sengupta, Coupling growth-factor engineering with nanotechnology for therapeutic angiogenesis. *Proc. Natl. Acad. Sci. U. S. A.* **107**, 13608–13 (2010).
49. F. Andres, L. Iamele, T. Meyer, J. C. Stüber, F. Kast, E. Gherardi, H. H. Niemann, A. Plückthun,

Inhibition of the MET Kinase Activity and Cell Growth in MET-Addicted Cancer Cells by Bi-Paratopic Linking. *J. Mol. Biol.* **431**, 2020–2039 (2019).

50. A. Louvet, F. Teixeira-Clerc, M.-N. Chobert, V. Deveaux, C. Pavoine, A. Zimmer, F. Pecker, A. Mallat, S. Lotersztajn, Cannabinoid CB2 receptors protect against alcoholic liver disease by regulating Kupffer cell polarization in mice. *Hepatology* **54**, 1217–1226 (2011).
51. T. Nakamura, H. Teramoto, A. Ichihara, Purification and characterization of a growth factor from rat platelets for mature parenchymal hepatocytes in primary cultures. *Proc. Natl. Acad. Sci. U. S. A.* **83**, 6489–93 (1986).
52. S. Mizuno, T. Nakamura, Hepatocyte growth factor: a regenerative drug for acute hepatitis and liver cirrhosis. *Regen. Med.* **2**, 161–70 (2007).
53. K. Horiguchi, A. E. Tadamichi, H. Ae, T. Ueki, A. E. Kazuhide, H. Ae, J. Fujimoto, Treating liver cirrhosis in dogs with hepatocyte growth factor gene therapy via the hepatic artery (2009) https:/doi.org/10.1007/s00534-008-0029-7.
54. T. Ueki, Y. Kaneda, H. Tsutsui, K. Nakanishi, Y. Sawa, R. Morishita, K. Matsumoto, T. Nakamura, H. Takahashi, E. Okamoto, J. Fujimoto, Hepatocyte growth factor gene therapy of liver cirrhosis in rats. *Nat. Med.* **5**, 226–230 (1999).
55. S. H. Moon, C. M. Lee, S.-H. Park, M. Jin Nam, Effects of hepatocyte growth factor gene-transfected mesenchymal stem cells on dimethylnitrosamine-induced liver fibrosis in rats. *Growth Factors* **37**, 105–119 (2019).
56. M. Cassano, S. Biressi, A. Finan, L. Benedetti, C. Omes, R. Boratto, F. Martin, M. Allegretti, V. Broccoli, G. Cusella De Angelis, P. M. Comoglio, C. Basilico, Y. Torrente, P. Michieli, G. Cossu, M. Sampaolesi, Magic-factor 1, a partial agonist of Met, induces muscle hypertrophy by protecting myogenic progenitors from apoptosis. *PLoS One* **3**, e3223 (2008).
57. C. J. Liu, D. S. Jones, P. Tsai, A. Venkataramana, J. R. Cochran, An engineered dimeric fragment of hepatocyte growth factor is a potent c-MET agonist. *FEBS Lett.* **588**, 4831–4837 (2014).
58. Y. C. Kim, J. Lee, J. N. An, J. H. Kim, Y. W. Choi, L. Li, S. H. Kwon, M. Y. Lee, B. Lee, J. G. Jeong, S. S. Yu, C. S. Lim, Y. S. Kim, S. Kim, S. H. Yang, J. P. Lee, Renoprotective effects of a novel cMet agonistic antibody on kidney fibrosis. *Sci. Rep.* **9**, 1–12 (2019).
59. S. Gallo, S. Gatti, V. Sala, R. Albano, P. Costelli, E. Casanova, P. M. Comoglio, T. Crepaldi, Agonist antibodies activating the Met receptor protect cardiomyoblasts from cobalt chloride-induced apoptosis and autophagy. *Cell Death Dis.* **5**, e1185-12 (2014).
60. H. Sato, R. Imamura, H. Suga, K. Matsumoto, K. Sakai, Cyclic Peptide-Based Biologics Regulating HGF-MET. *Int. J. Mol. Sci.* **21**, 7977 (2020).
61. R. Ueki, S. Uchida, N. Kanda, N. Yamada, A. Ueki, M. Akiyama, K. Toh, H. Cabral, S. Sando, A chemically unmodified agonistic DNA with growth factor functionality for in vivo therapeutic application. *Sci. Adv.* **6**, 1–12 (2020).
62. M. Tahara, K. Matsumoto, T. Nukiwa, T. Nakamura, Hepatocyte growth factor leads to recovery from alcohol-induced fatty liver in rats. *J. Clin. Invest.* **103**, 313–320 (1999).
63. Y. Matsuda, K. Matsumoto, T. Nakamura, T. Ichida, Hepatocyte growth factor suppresses the onset of liver cirrhosis and abrogates lethal hepatic dysfunction in rats. *J. Biochem.* **118**, 643–649 (1995).
64. M. De Rosa, D. Rega, V. Costabile, F. Duraturo, A. Niglio, P. Izzo, U. Pace, P. Delrio, The biological complexity of colorectal cancer: insights into biomarkers for early detection and personalized care. *Therap. Adv. Gastroenterol.* **9**, 861–886 (2016).
65. J. Taïeb, C. Delarche, V. Paradis, P. Mathurin, A. Grenier, B. Crestani, M. Dehoux, D. Thabut, M.-A. Gougerot-Pocidalo, T. Poynard, S. Chollet-Martin, Polymorphonuclear neutrophils are a source of

hepatocyte growth factor in patients with severe alcoholic hepatitis. *J. Hepatol.* **36**, 342–348 (2002).

66. Y. Matsuda, Preventive and therapeutic effects in rats of hepatocyte growth factor infusion on liver fibrosis/cirrhosis. *Hepatology* **26**, 81–89 (1997).

67. D. C. Kroy, F. Schumacher, P. Ramadori, M. Hatting, I. Bergheim, N. Gassler, M. V. Boekschoten, M. Müller, K. L. Streetz, C. Trautwein, Hepatocyte specific deletion of c-Met leads to the development of severe non-alcoholic steatohepatitis in mice. *J. Hepatol.* **61**, 883–890 (2014).

68. A. Ishigaki, M. Aoki, M. Nagai, H. Warita, S. Kato, M. Kato, T. Nakamura, H. Funakoshi, Y. Itoyama, Intrathecal delivery of hepatocyte growth factor from amyotrophic lateral sclerosis onset suppresses disease progression in rat amyotrophic lateral sclerosis model. *J. Neuropathol. Exp. Neurol.* **66**, 1037–44 (2007).

69. S. H. Lee, S. Kim, N. Lee, J. Lee, S. S. Yu, J. H. Kim, S. Kim, Intrathecal delivery of recombinant AAV1 encoding hepatocyte growth factor improves motor functions and protects neuromuscular system in the nerve crush and SOD1-G93A transgenic mouse models. *Acta Neuropathol. Commun.* **7**, 96 (2019).

70. L. Bai, D. P. Lennon, A. I. Caplan, A. DeChant, J. Hecker, J. Kranso, A. Zaremba, R. H. Miller, Hepatocyte growth factor mediates mesenchymal stem cell–induced recovery in multiple sclerosis models. *Nat. Neurosci.* **15**, 862–870 (2012).

71. A. Vallarola, M. Tortarolo, R. De Gioia, L. Iamele, H. de Jonge, G. de Nola, E. Bovio, L. Pasetto, V. Bonetto, M. Freschi, C. Bendotti, E. Gherardi, A Novel HGF/SF Receptor (MET) Agonist Transiently Delays the Disease Progression in an Amyotrophic Lateral Sclerosis Mouse Model by Promoting Neuronal Survival and Dampening the Immune Dysregulation. *Int. J. Mol. Sci.* **21**, 8542 (2020).

Figure 1

A

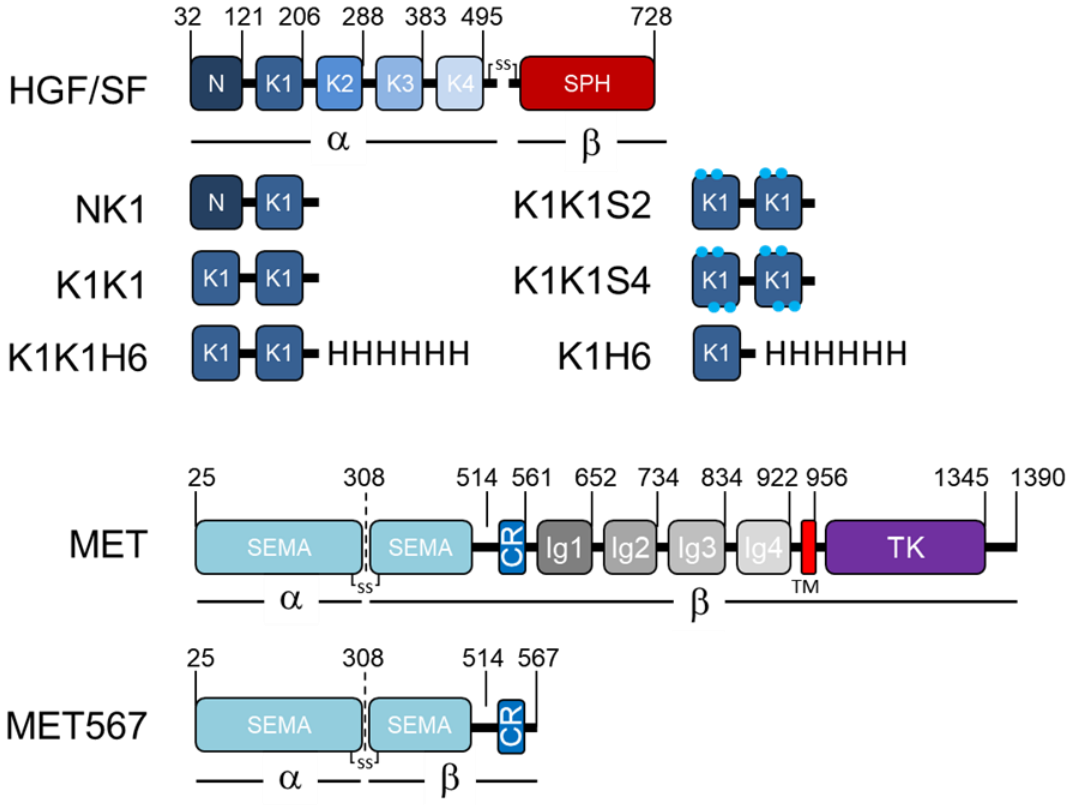

B

```
1          10          20          30          40          50          60
MAIRNCIIGK GRSYKGTVSI TKSGIKCQPW SSMIPHEHSF LPSSYRGKDL QENYCRNPRG
          70          80          90          100         110         120
EEGGPWCFTS NPEVRYEVCD IPQCSEVECI IGKGRSYKGT VSITKSGIKC QPWSSMIPHE
         130         140         150         160         170     177
HSFLPSSYRG KDLQENYCRN PRGEEGGPWC FTSNPEVRYE VCDIPQCSEV EHHHHHH
```

C

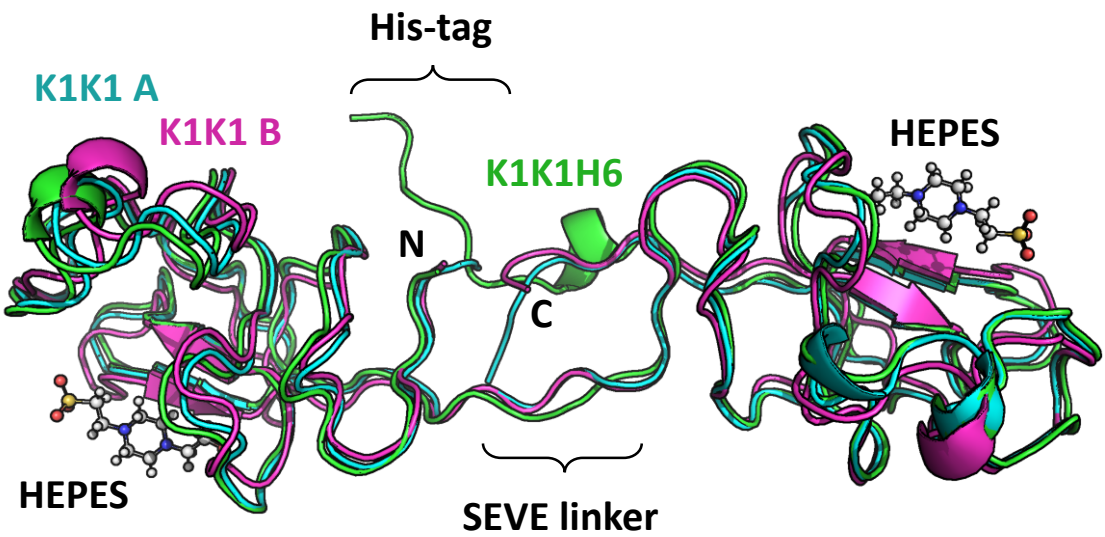

Figure 2

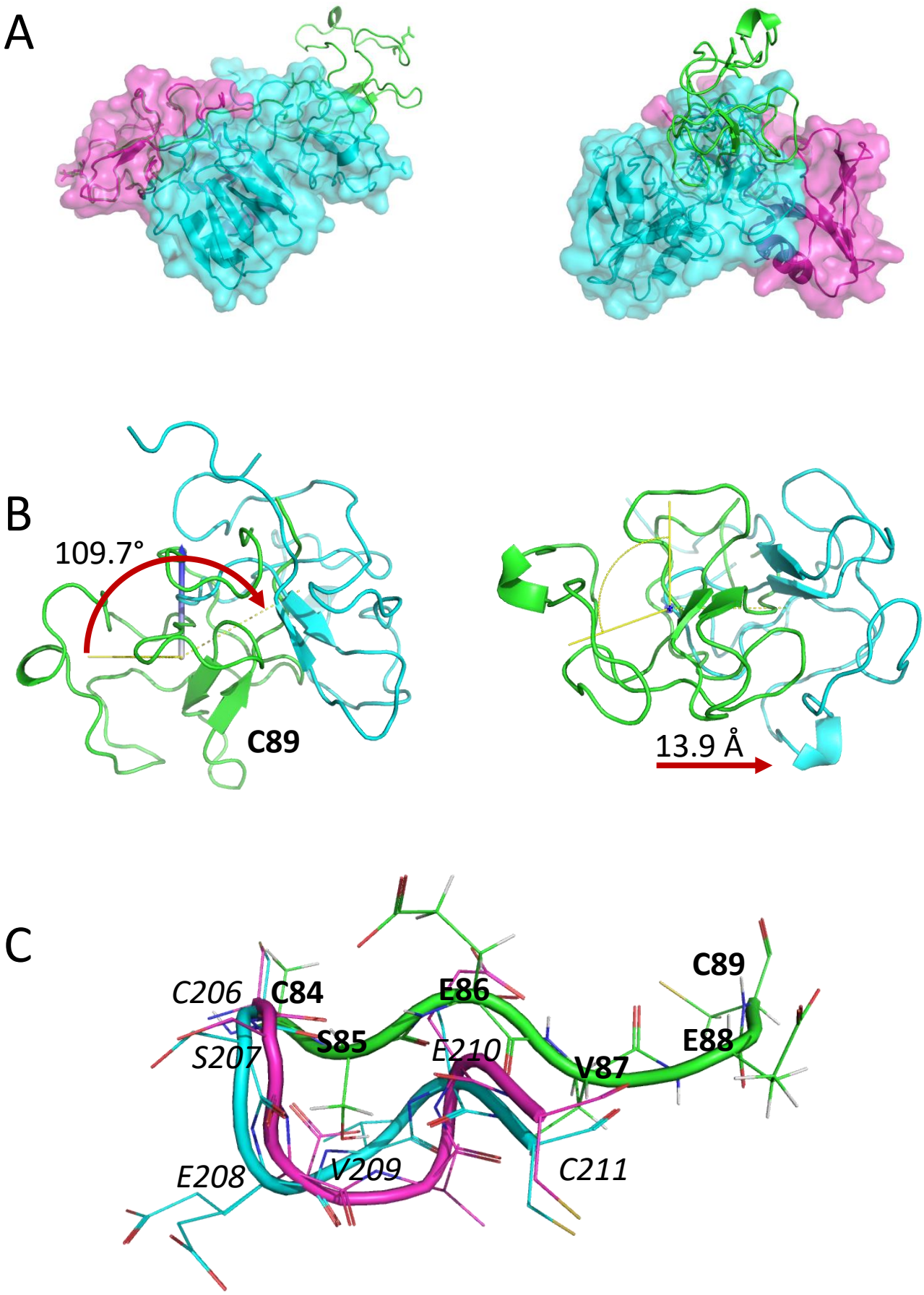
A
B
109.7°
C89
13.9 Å
C
C206
C84
E86
C89
S85
E210
E88
S207
V87
E208
V209
C211

Figure 3

A

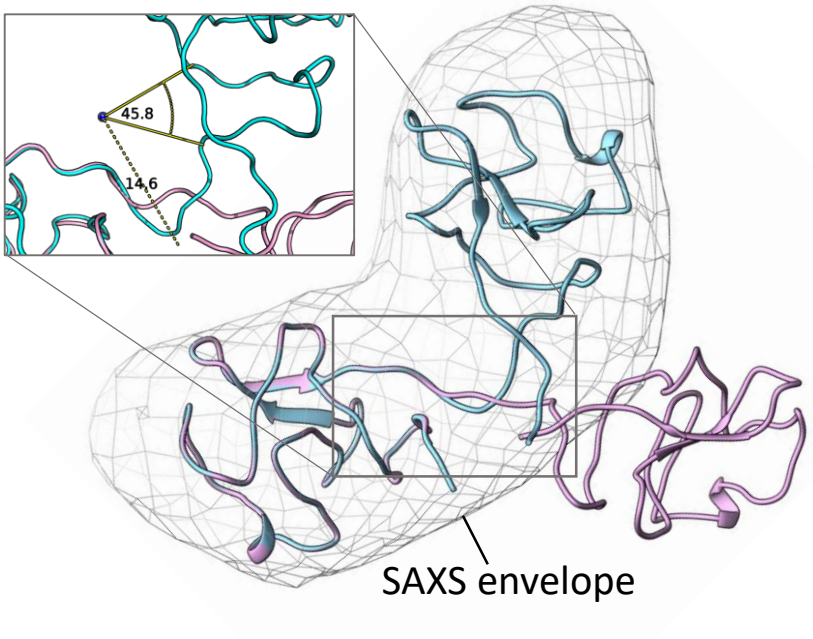
45.8
14.6
SAXS envelope

B

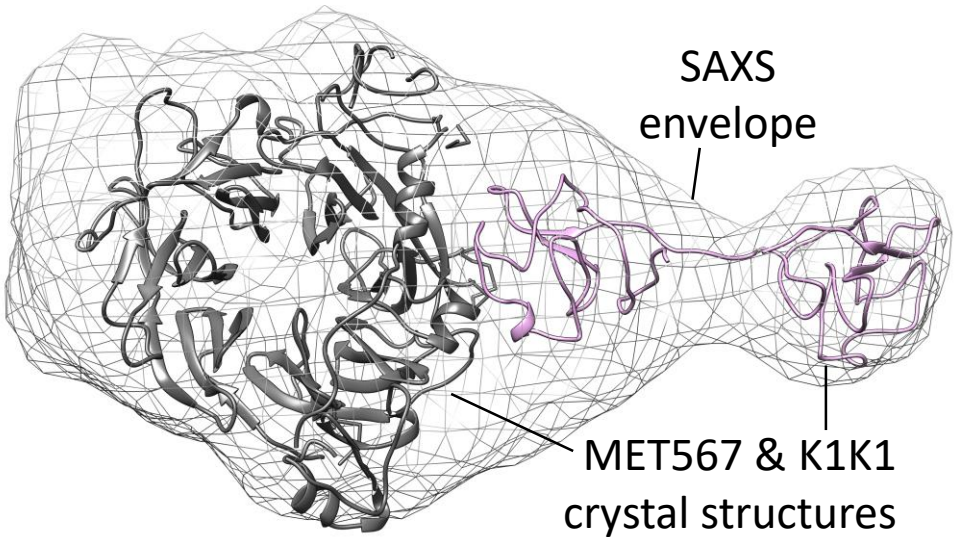
SAXS
envelope
MET567 & K1K1
crystal structures

Figure 4

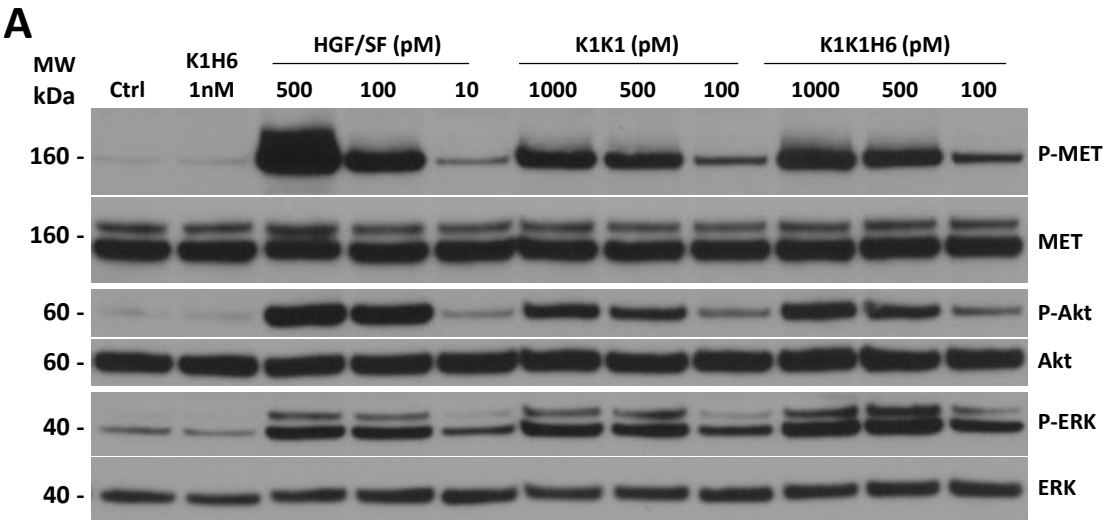
A
MW
kDa
Ctrl
K1H6
1nM
HGF/SF (pM)
500
100
10
K1K1 (pM)
1000
500
100
K1K1H6 (pM)
1000
500
100
160 -
160 -
60 -
60 -
40 -
40 -
P-MET
MET
P-Akt
Akt
P-ERK
ERK

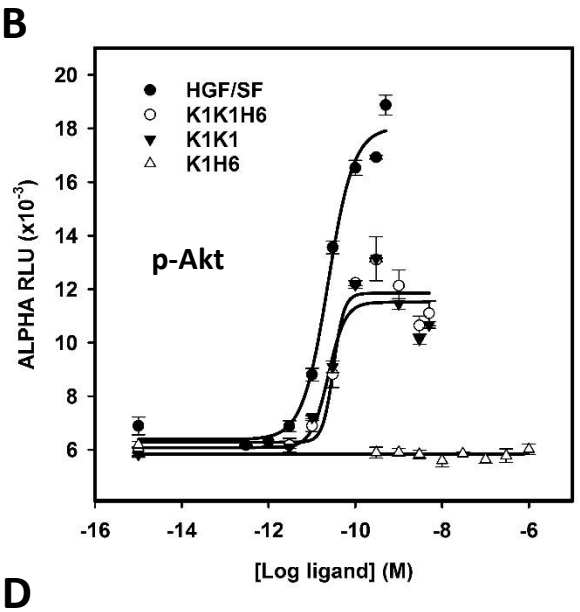
B
HGF/SF
K1K1H6
K1K1
K1H6
p-Akt
ALPHA RLU (x10-3)
[Log ligand] (M)

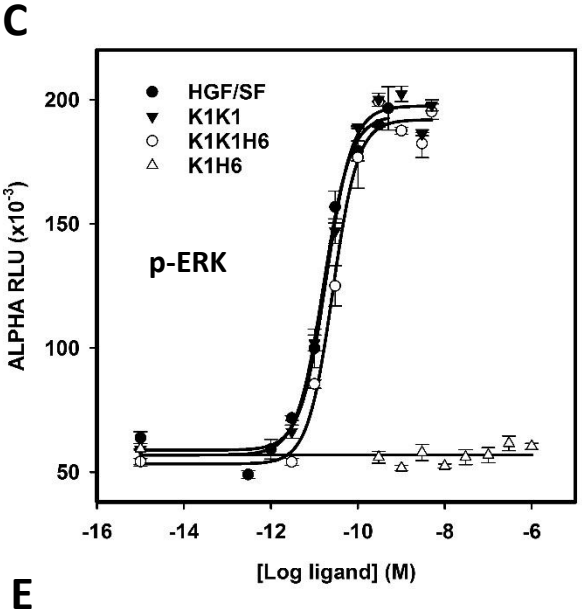
C
HGF/SF
K1K1
K1K1H6
K1H6
p-ERK
ALPHA RLU (x10-3)
[Log ligand] (M)

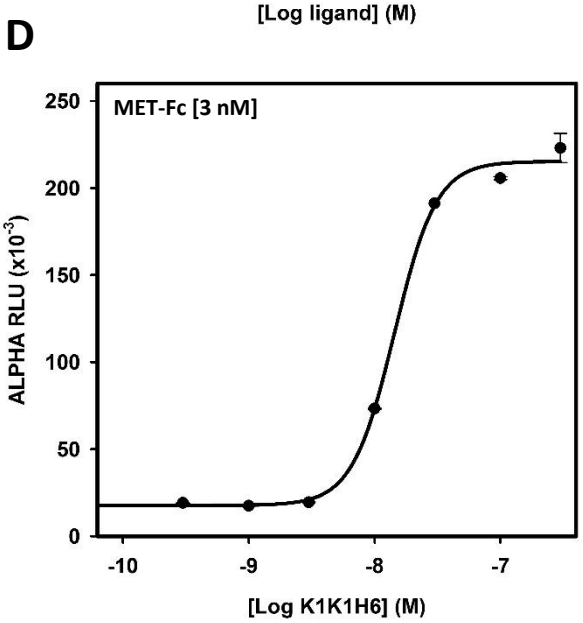
D
MET-Fc [3 nM]
ALPHA RLU (x10-3)
[Log K1K1H6] (M)

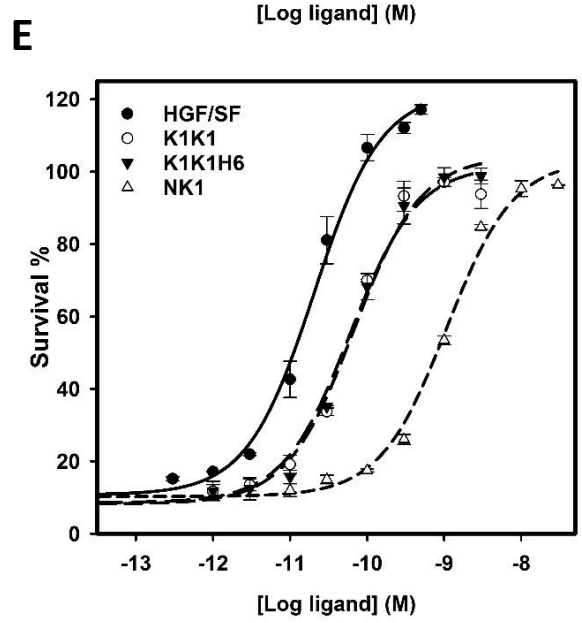
E
HGF/SF
K1K1
K1K1H6
NK1
Survival %
[Log ligand] (M)

Figure 5

A

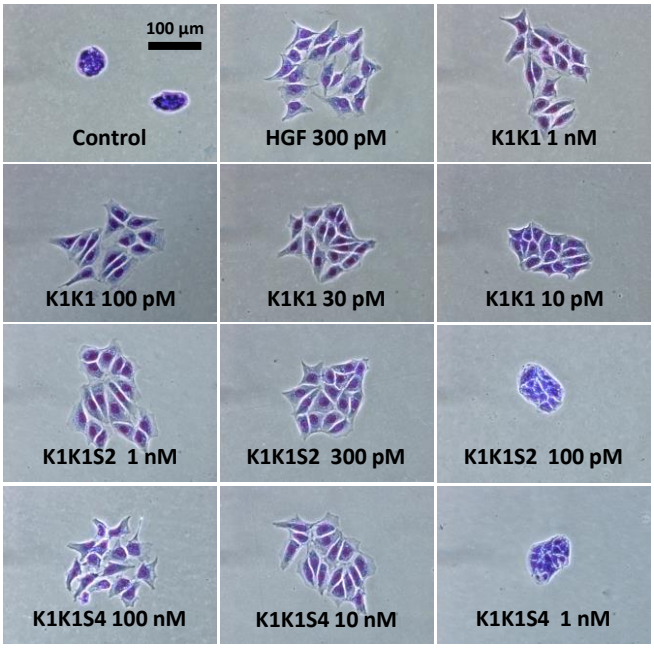
100 µm
Control
HGF 300 pM
K1K1 1 nM
K1K1 100 pM
K1K1 30 pM
K1K1 10 pM
K1K1S2 1 nM
K1K1S2 300 pM
K1K1S2 100 pM
K1K1S4 100 nM
K1K1S4 10 nM
K1K1S4 1 nM

B

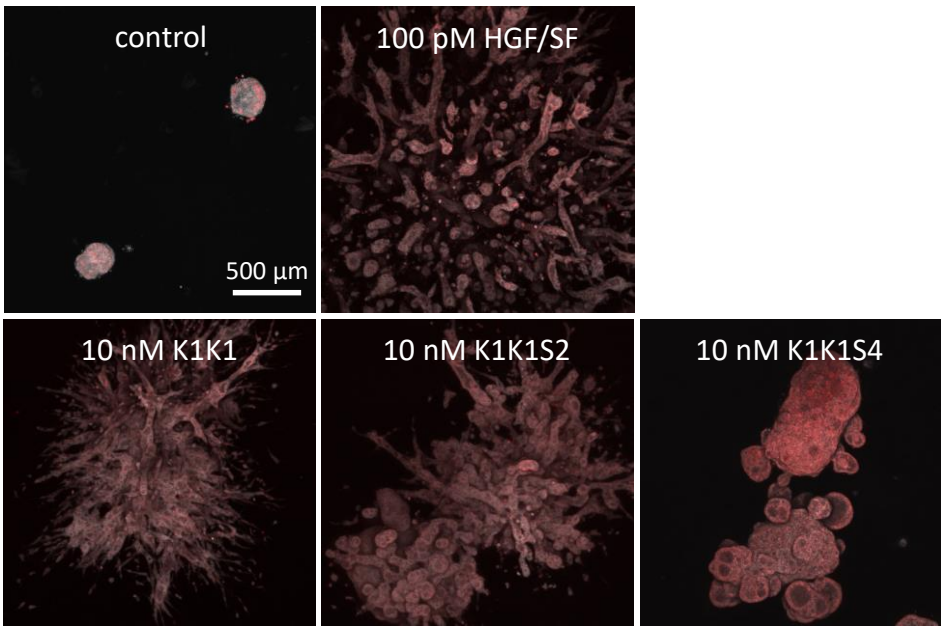
control
500 µm
100 pM HGF/SF
10 nM K1K1
10 nM K1K1S2
10 nM K1K1S4

C

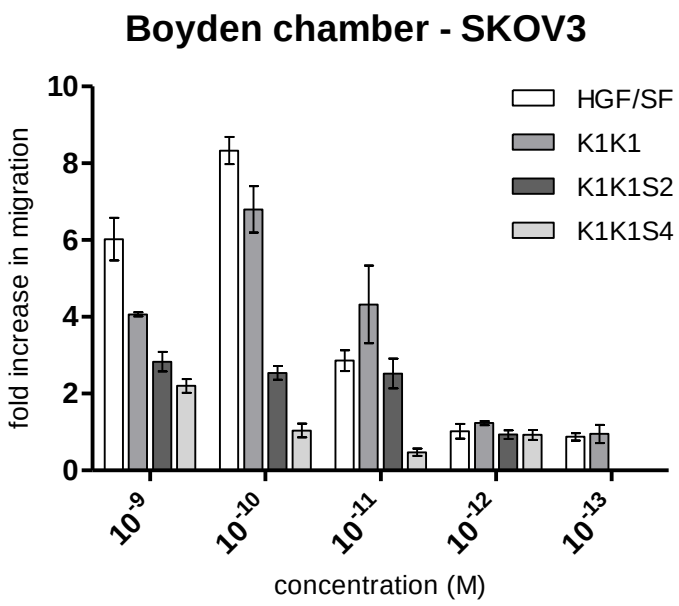
Boyden chamber - SKOV3
HGF/SF
K1K1
K1K1S2
K1K1S4
fold increase in migration
0
2
4
6
8
10
10-9
10-10
10-11
10-12
10-13
concentration (M)

Figure 6

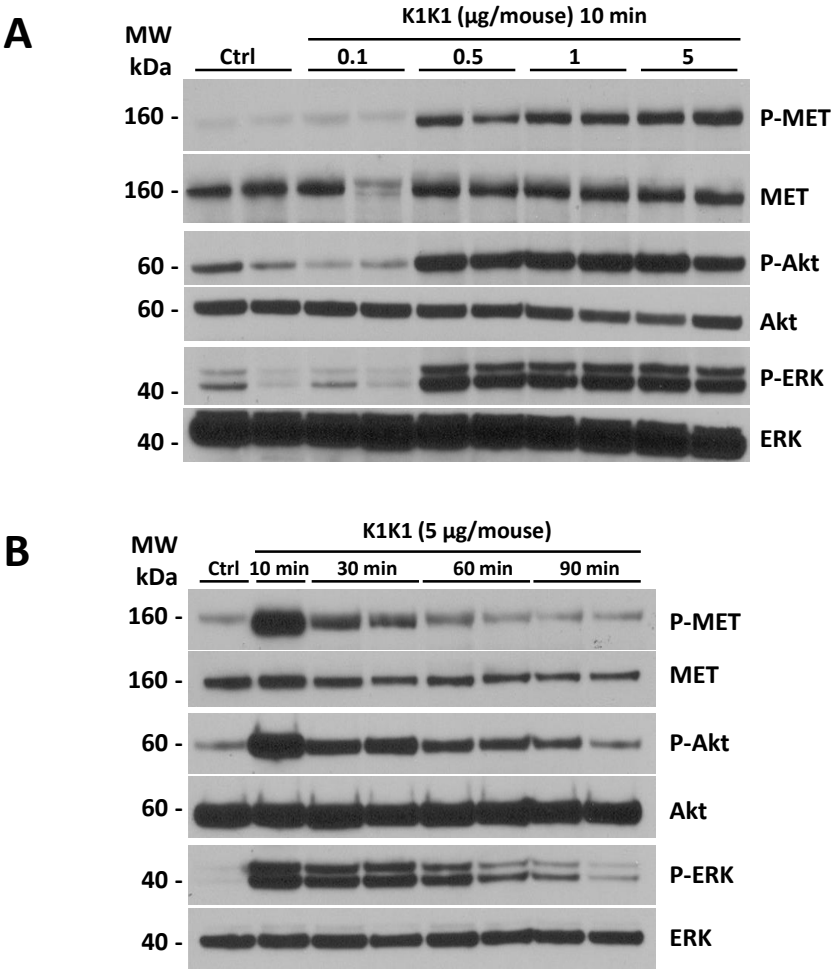
A
MW
kDa
K1K1 (µg/mouse) 10 min
Ctrl
0.1
0.5
1
5
160 -
P-MET
160 -
MET
60 -
P-Akt
60 -
Akt
40 -
P-ERK
40 -
ERK
B
MW
kDa
K1K1 (5 µg/mouse)
Ctrl
10 min
30 min
60 min
90 min
160 -
P-MET
160 -
MET
60 -
P-Akt
60 -
Akt
40 -
P-ERK
40 -
ERK

Figure 7

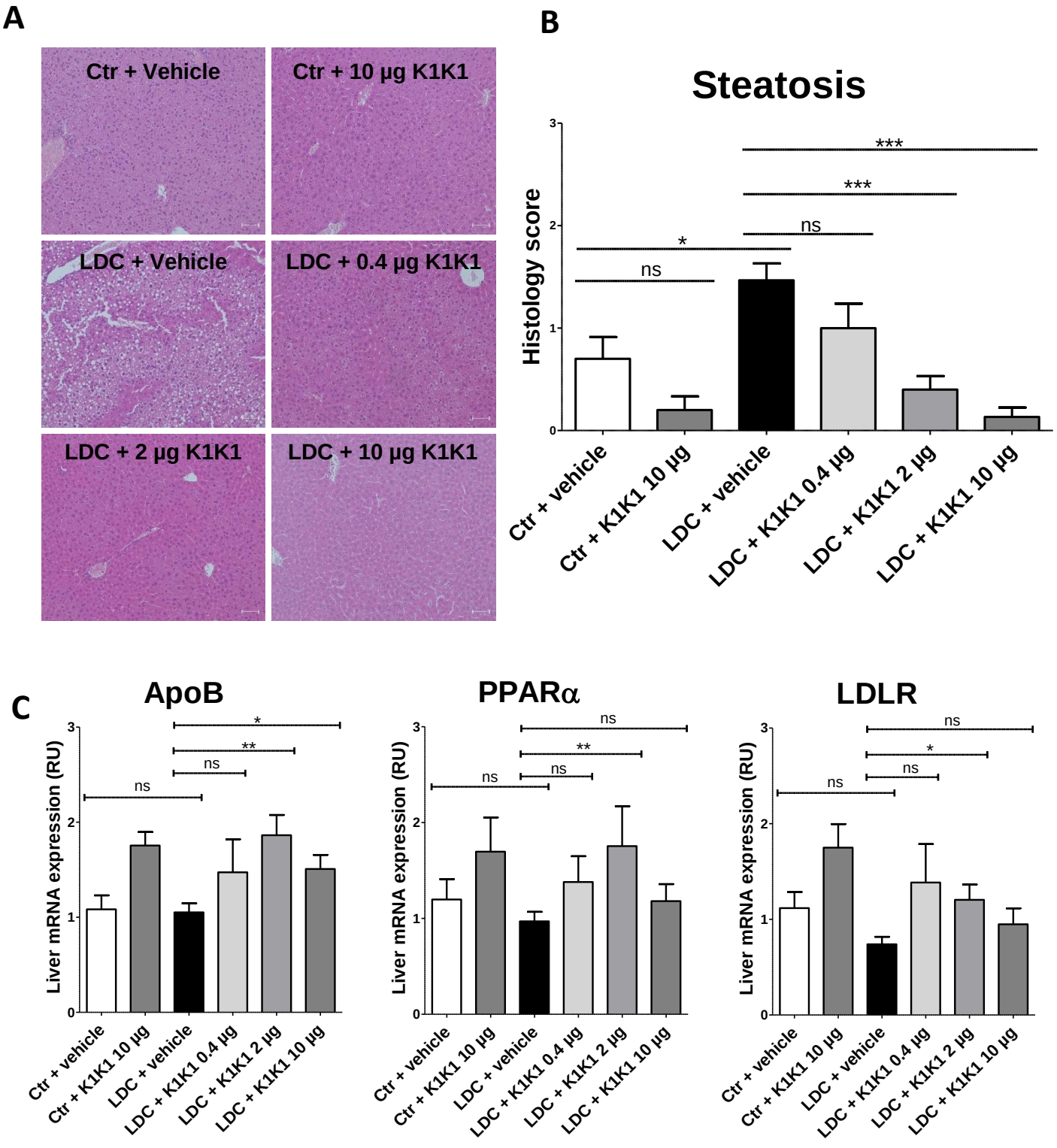
A
Ctr + Vehicle
Ctr + 10 µg K1K1
LDC + Vehicle
LDC + 0.4 µg K1K1
LDC + 2 µg K1K1
LDC + 10 µg K1K1
B
Steatosis
Histology score
0
1
2
3
ns
*
***
***
Ctr + vehicle
Ctr + K1K1 10 µg
LDC + vehicle
LDC + K1K1 0.4 µg
LDC + K1K1 2 µg
LDC + K1K1 10 µg
C
ApoB
PPARα
LDLR
Liver mRNA expression (RU)
0
1
2
3
ns
*
**
ns
Ctr + vehicle
Ctr + K1K1 10 µg
LDC + vehicle
LDC + K1K1 0.4 µg
LDC + K1K1 2 µg
LDC + K1K1 10 µg

Supplementary figure S1

A

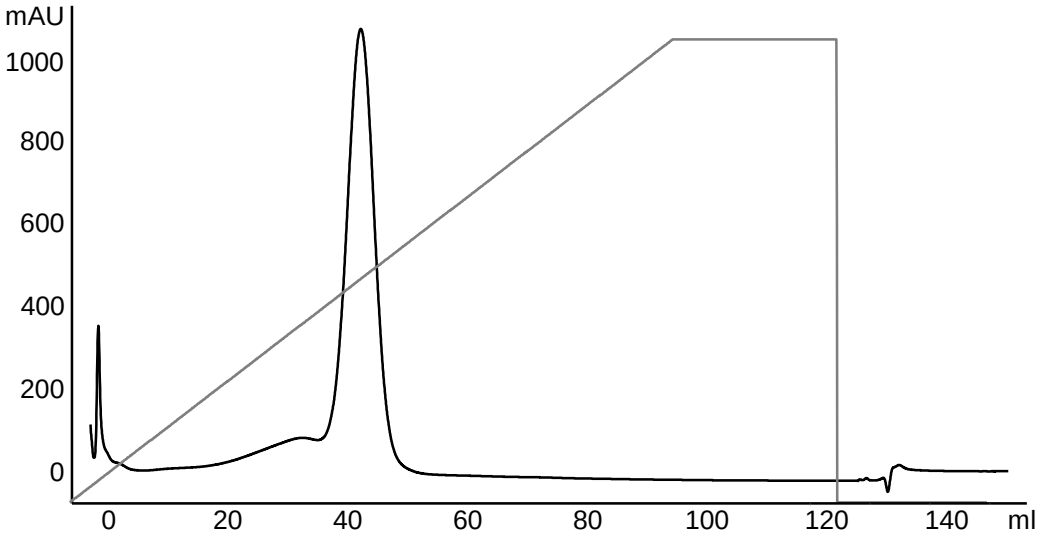

B

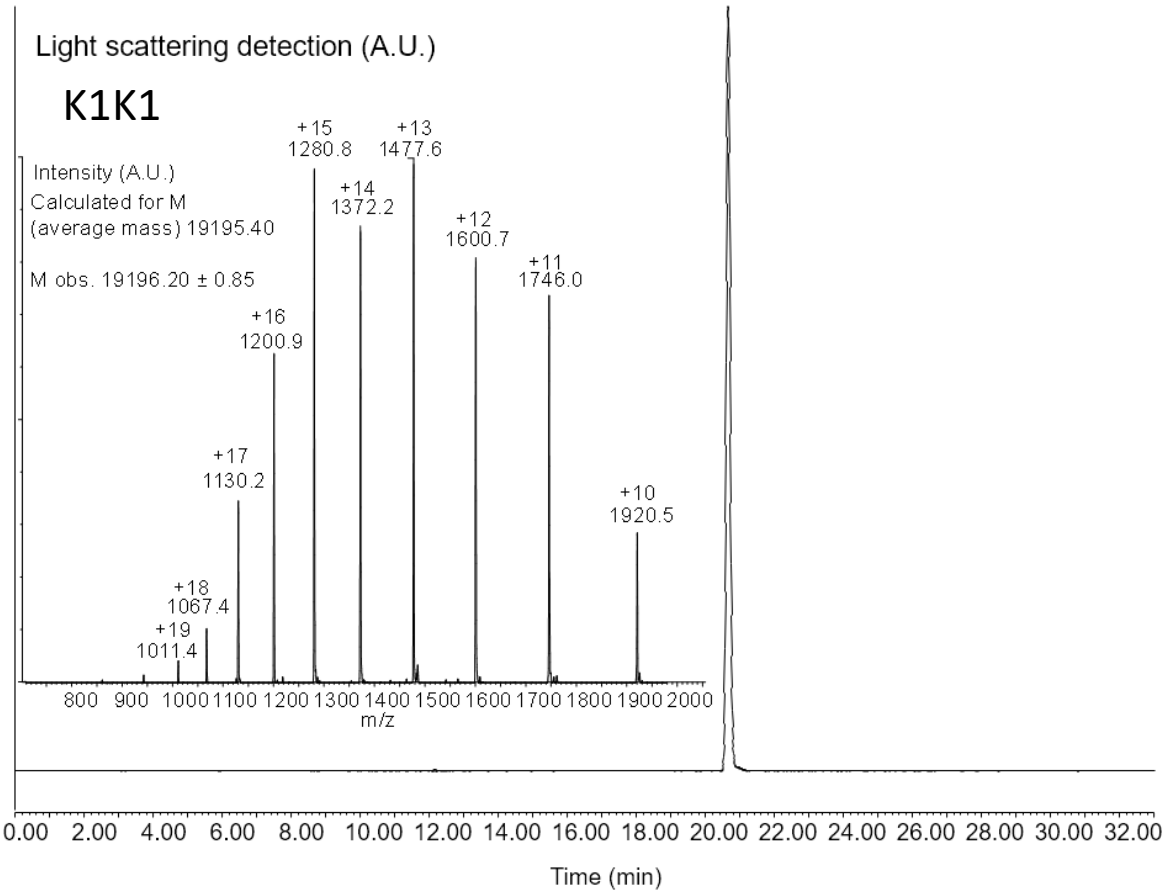

Supplementary figure S1

C

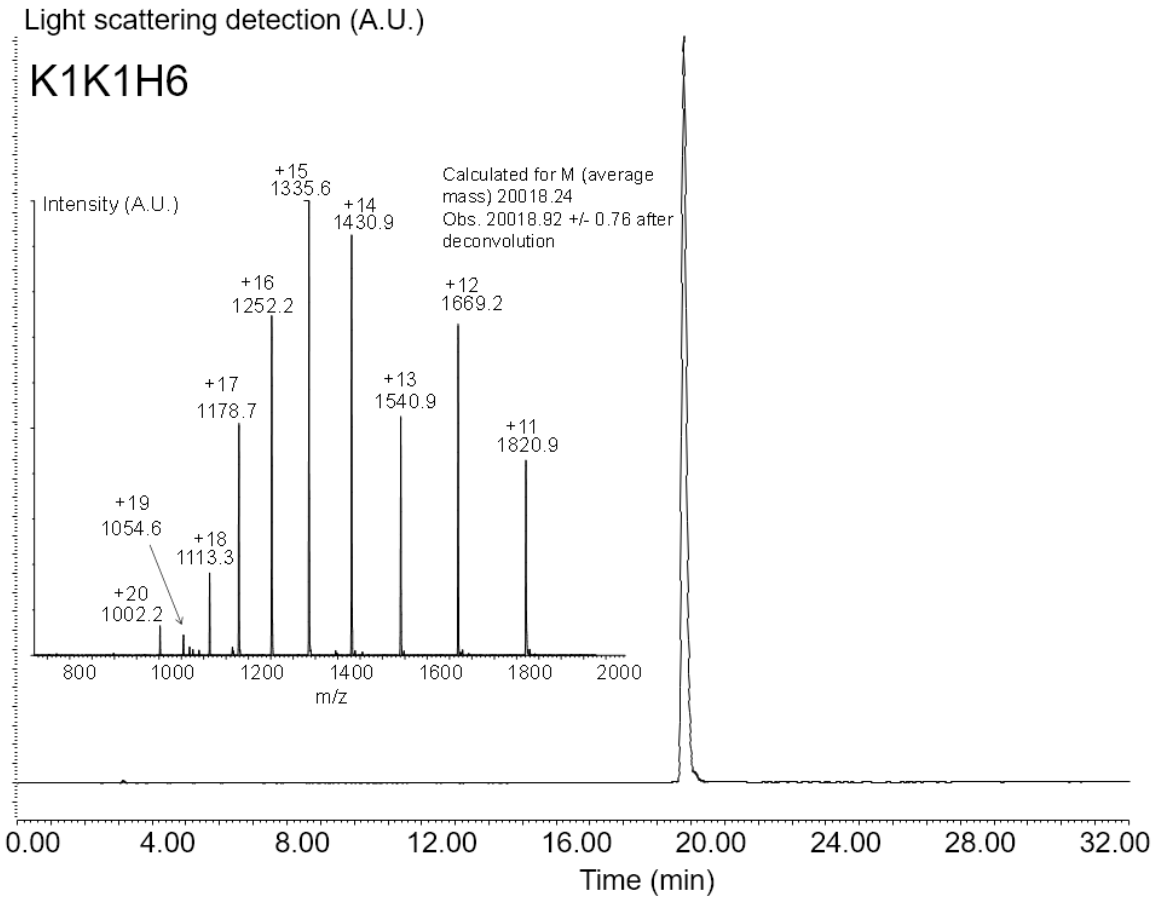

D

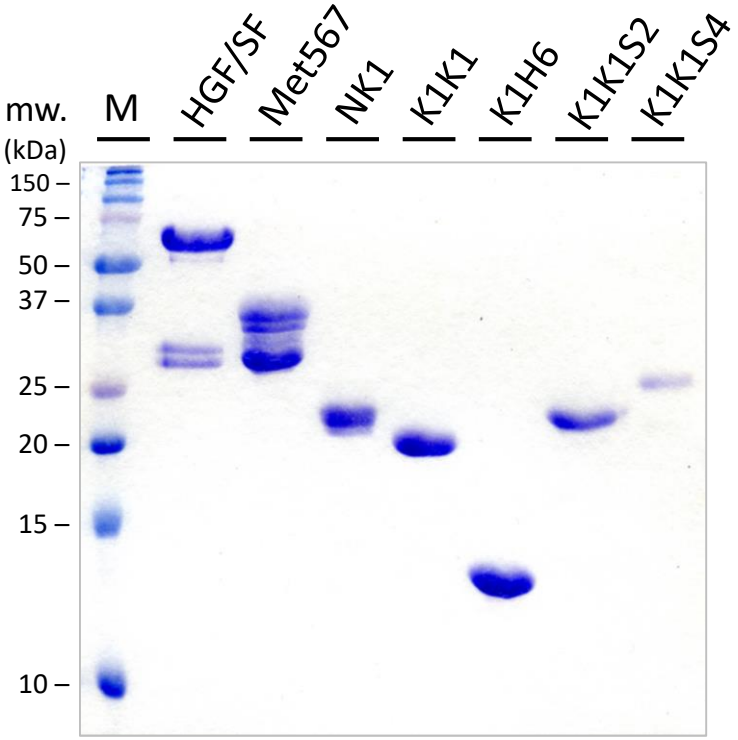

Supplementary figure S2

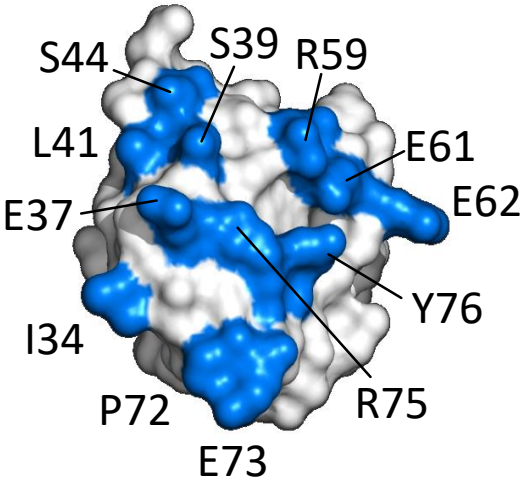

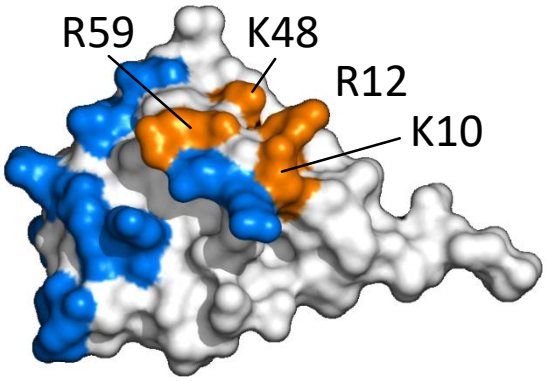

Supplementary figure S3

A

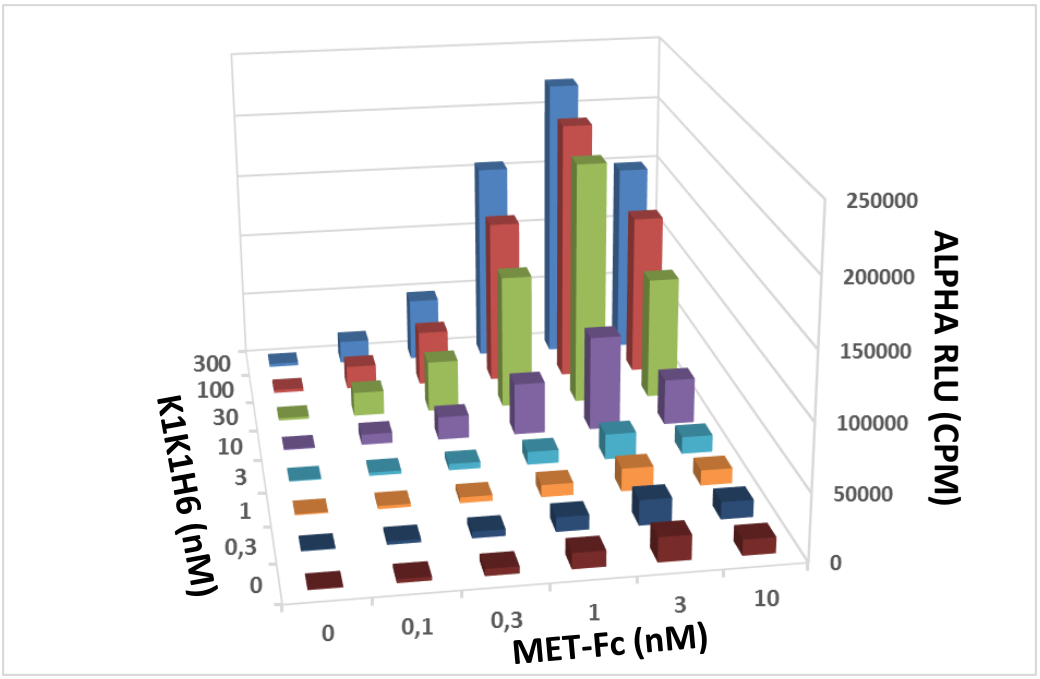

B

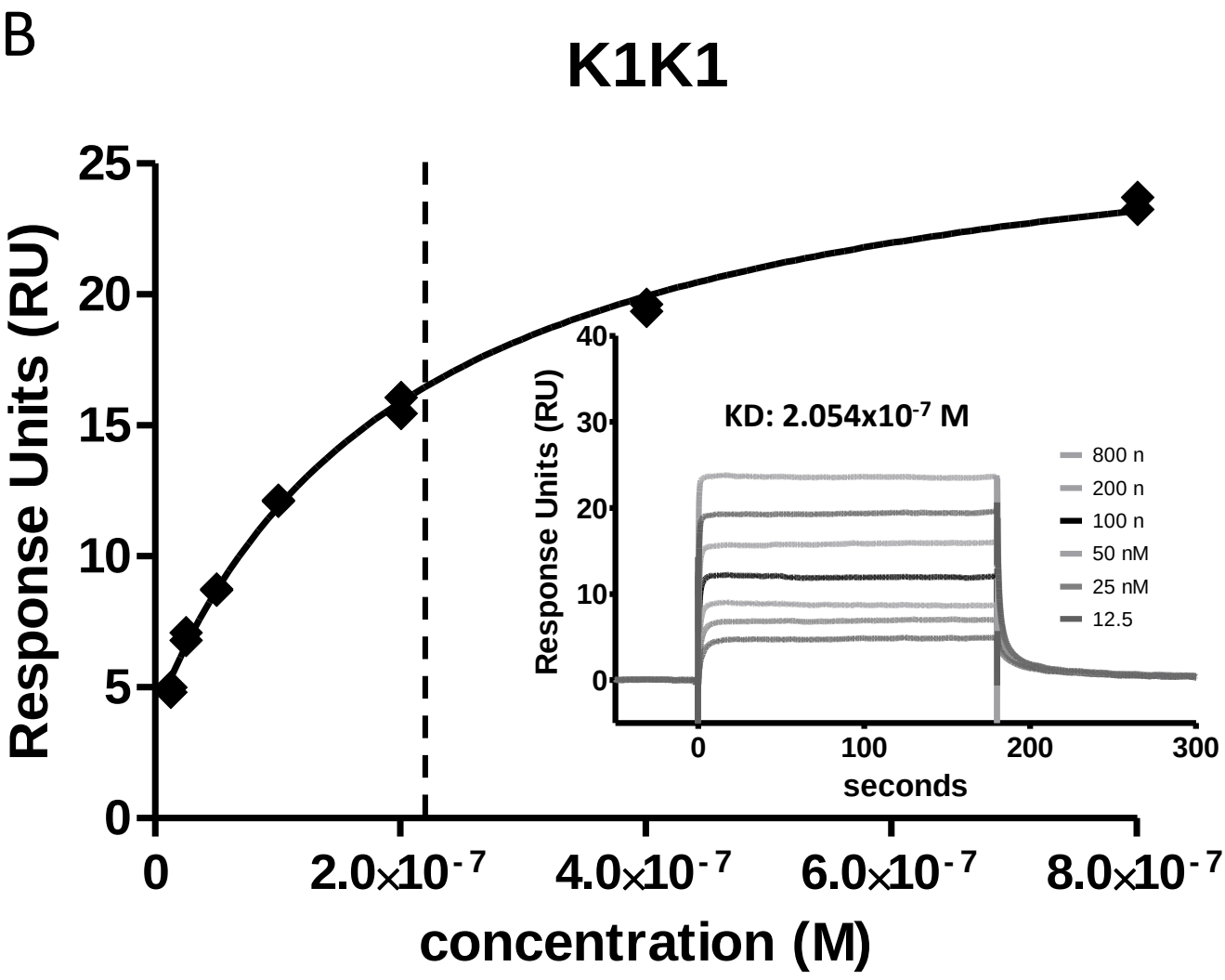

Supplementary figure S3

C

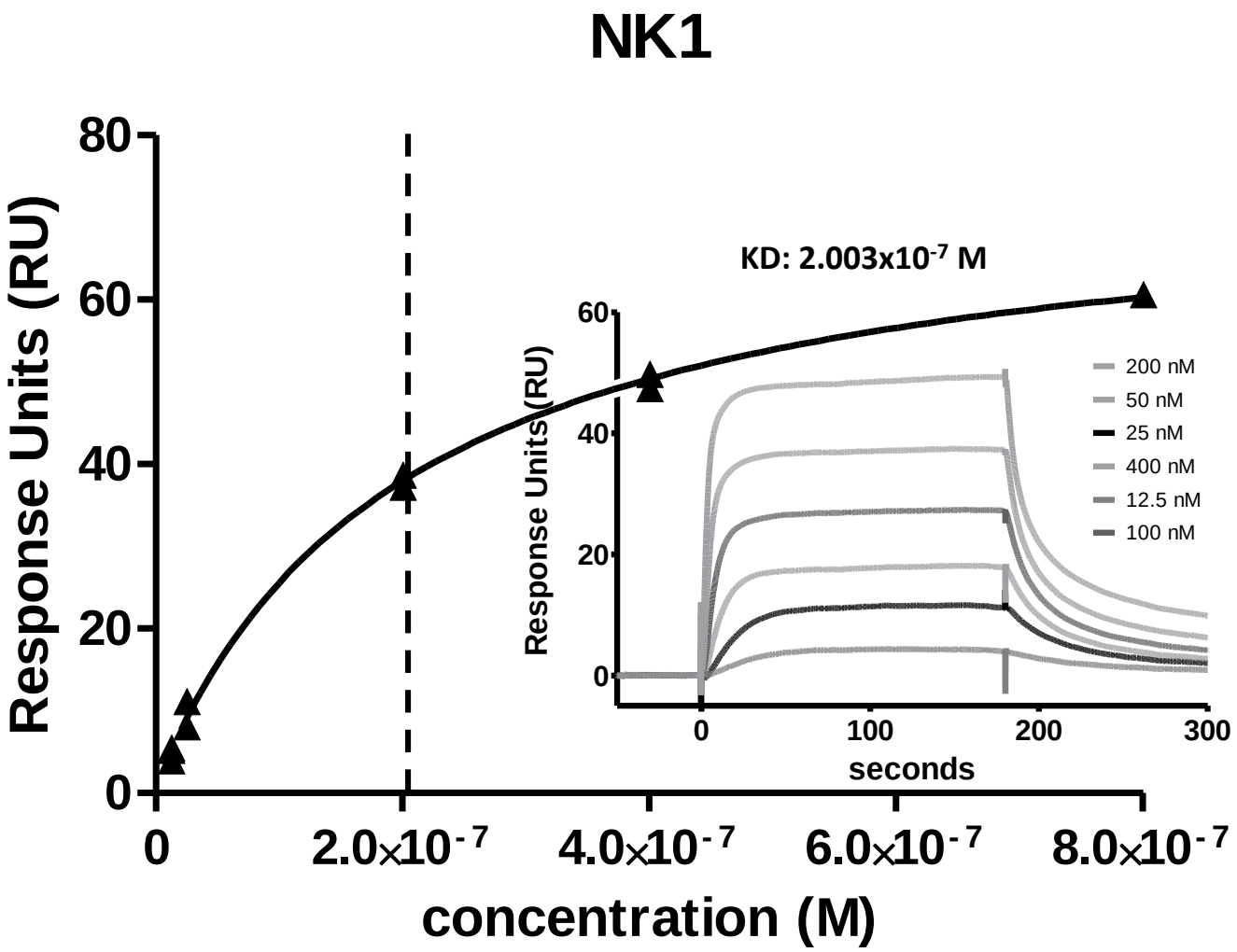

Supplementary figure S4

A

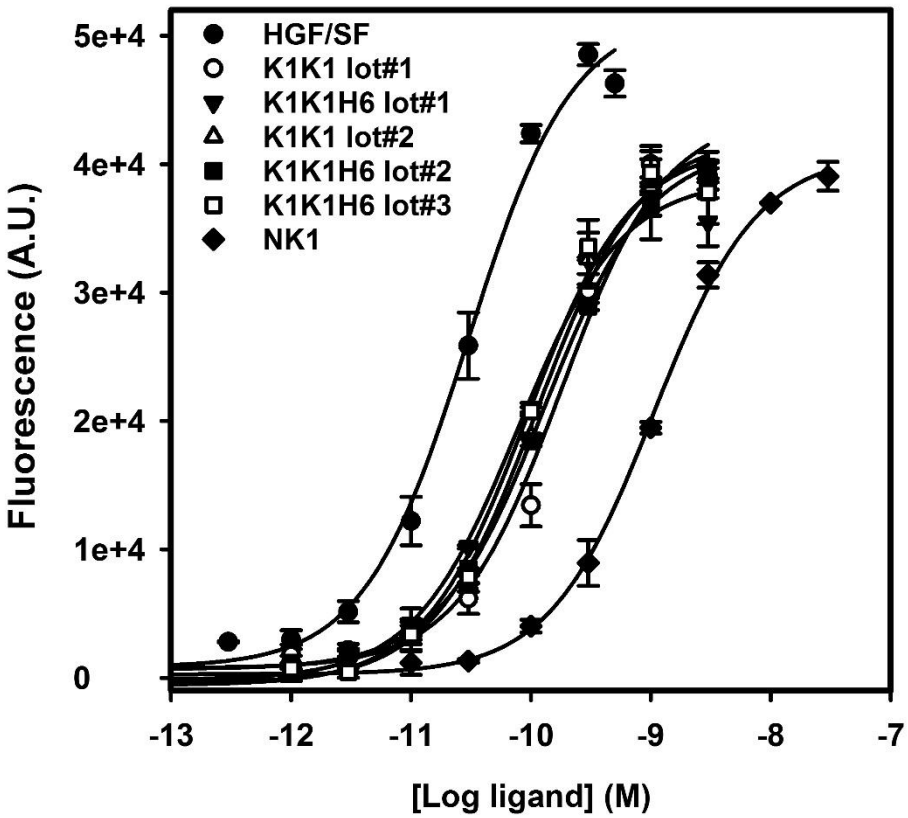

B

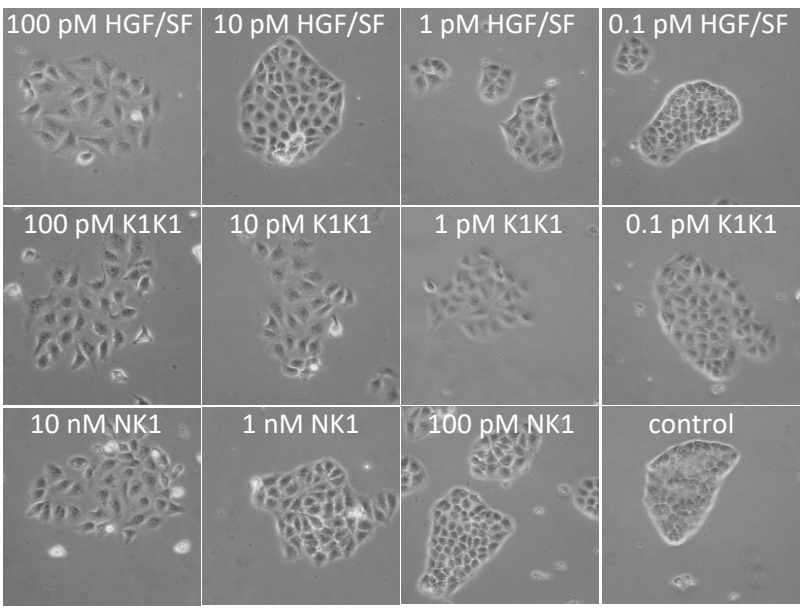

Supplementary figure S5

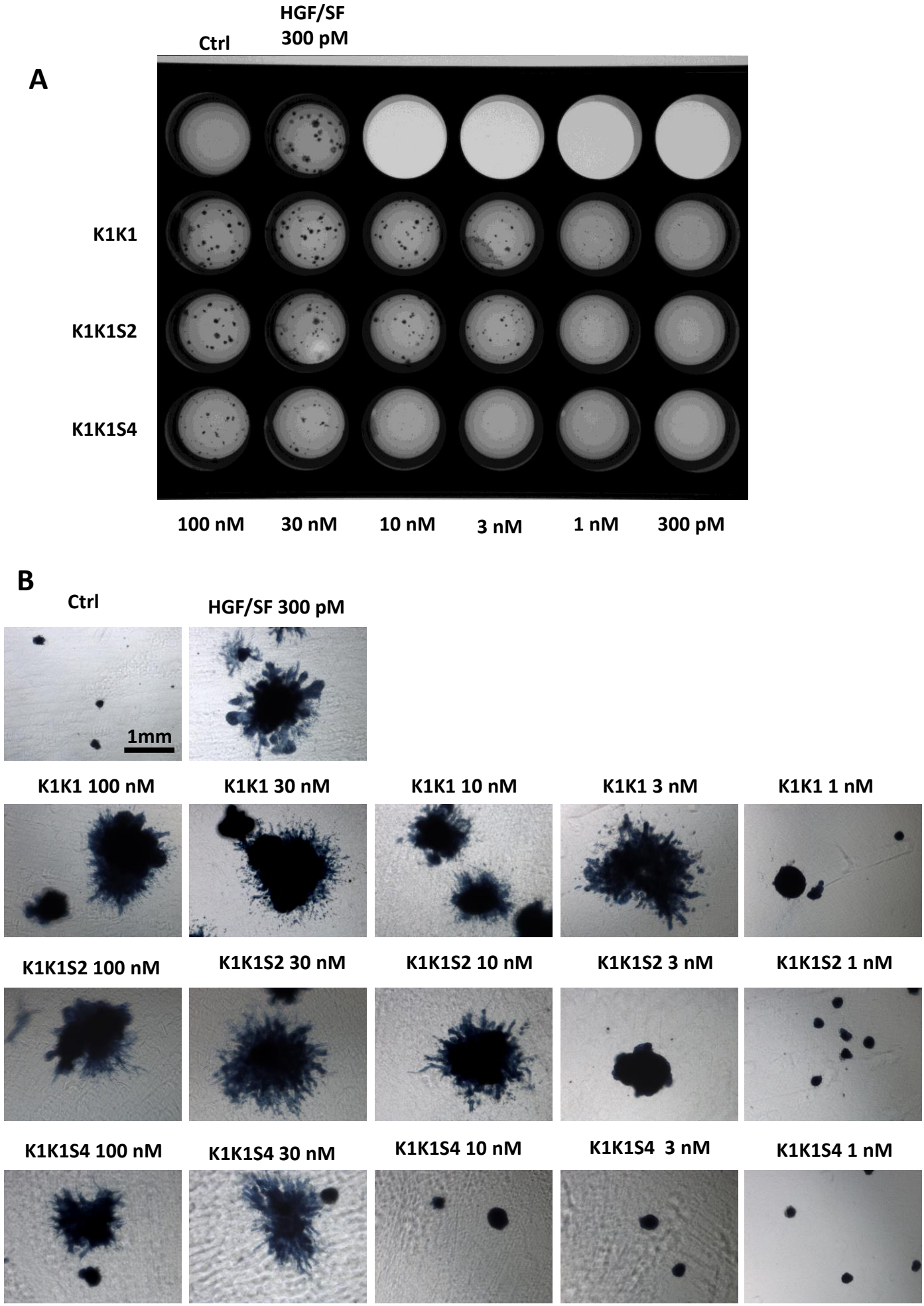

Supplementary figure S5

C

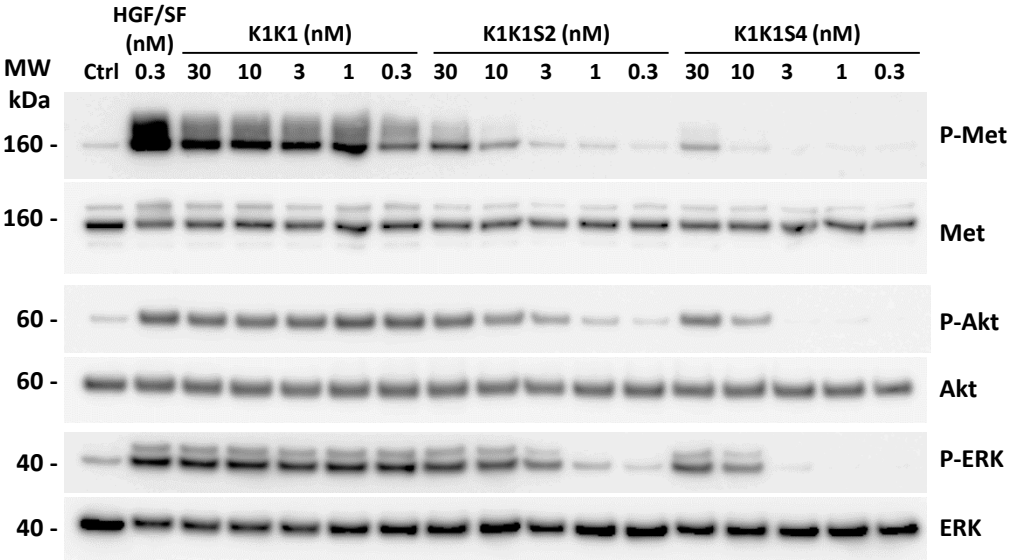

Supplementary figure S6

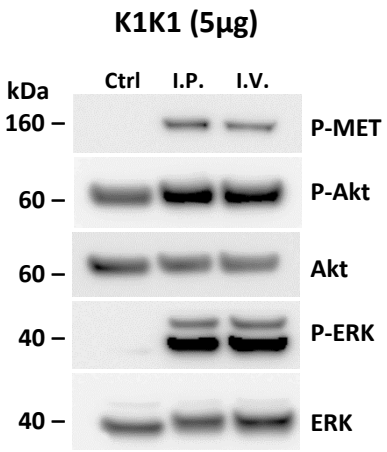

Supplementary figure S7

A

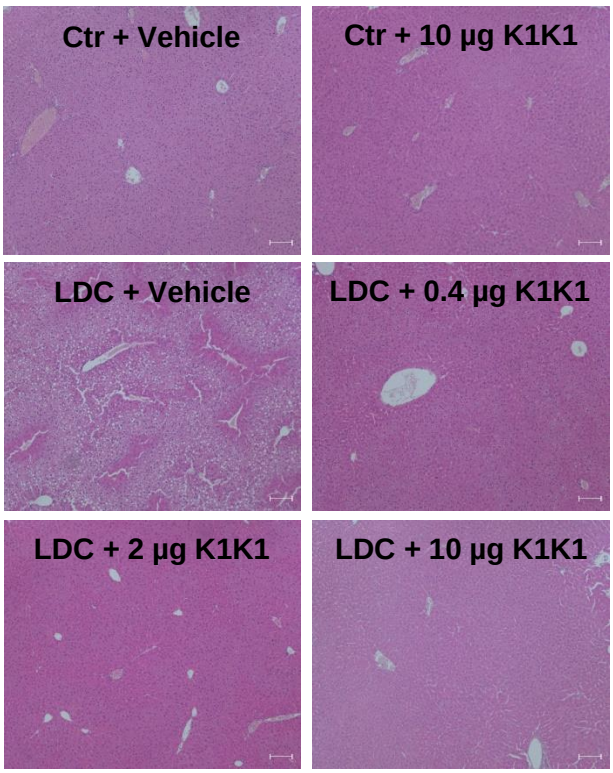

B

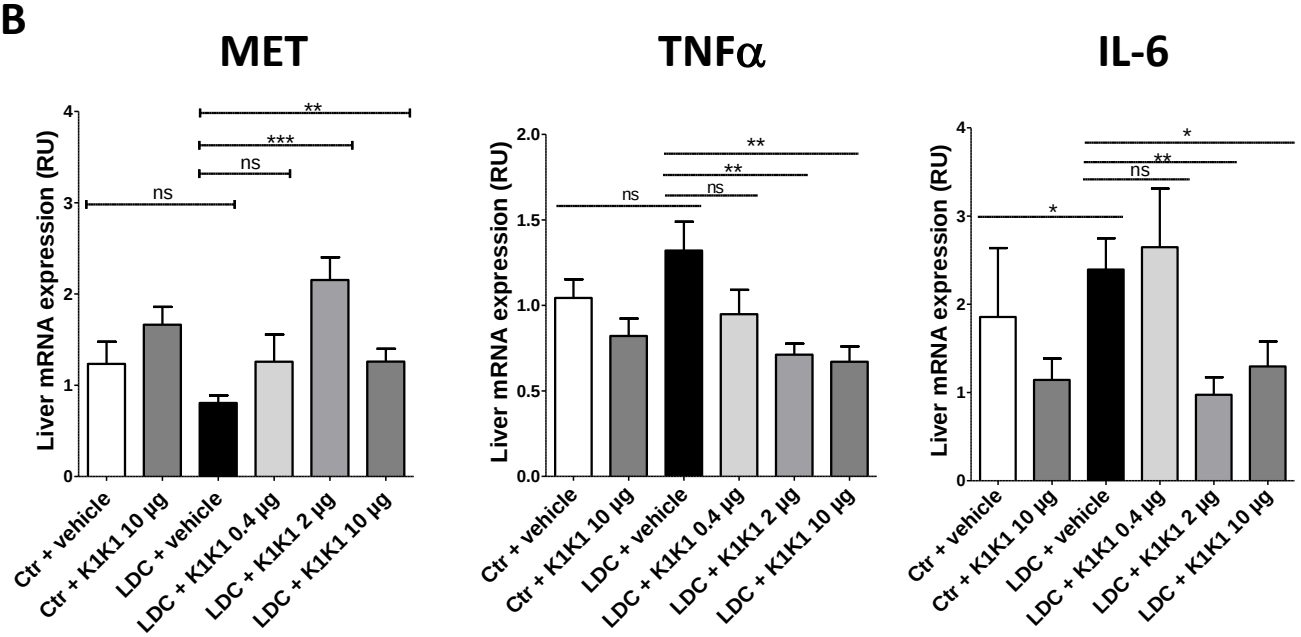

Supplementary figure S8

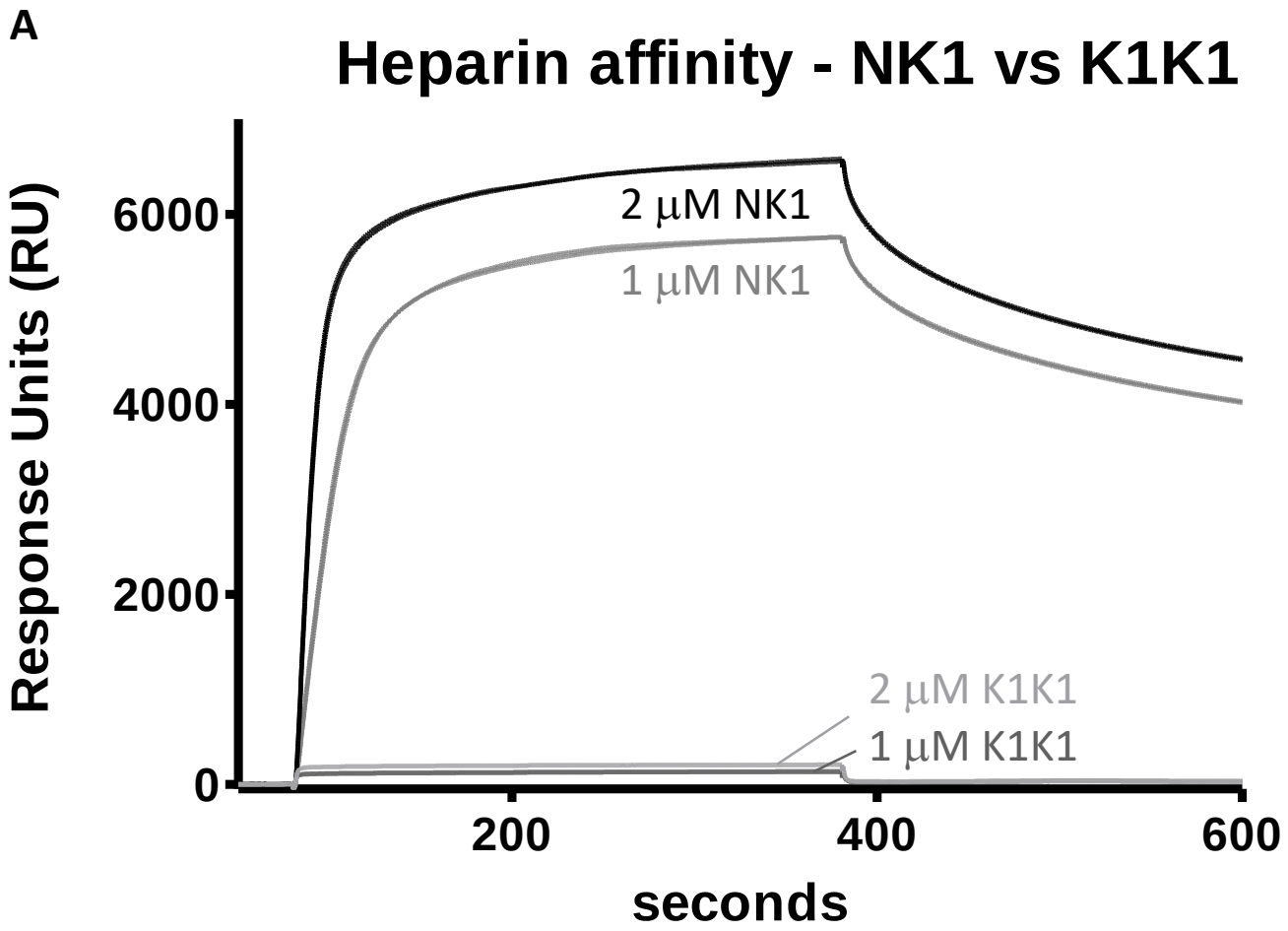

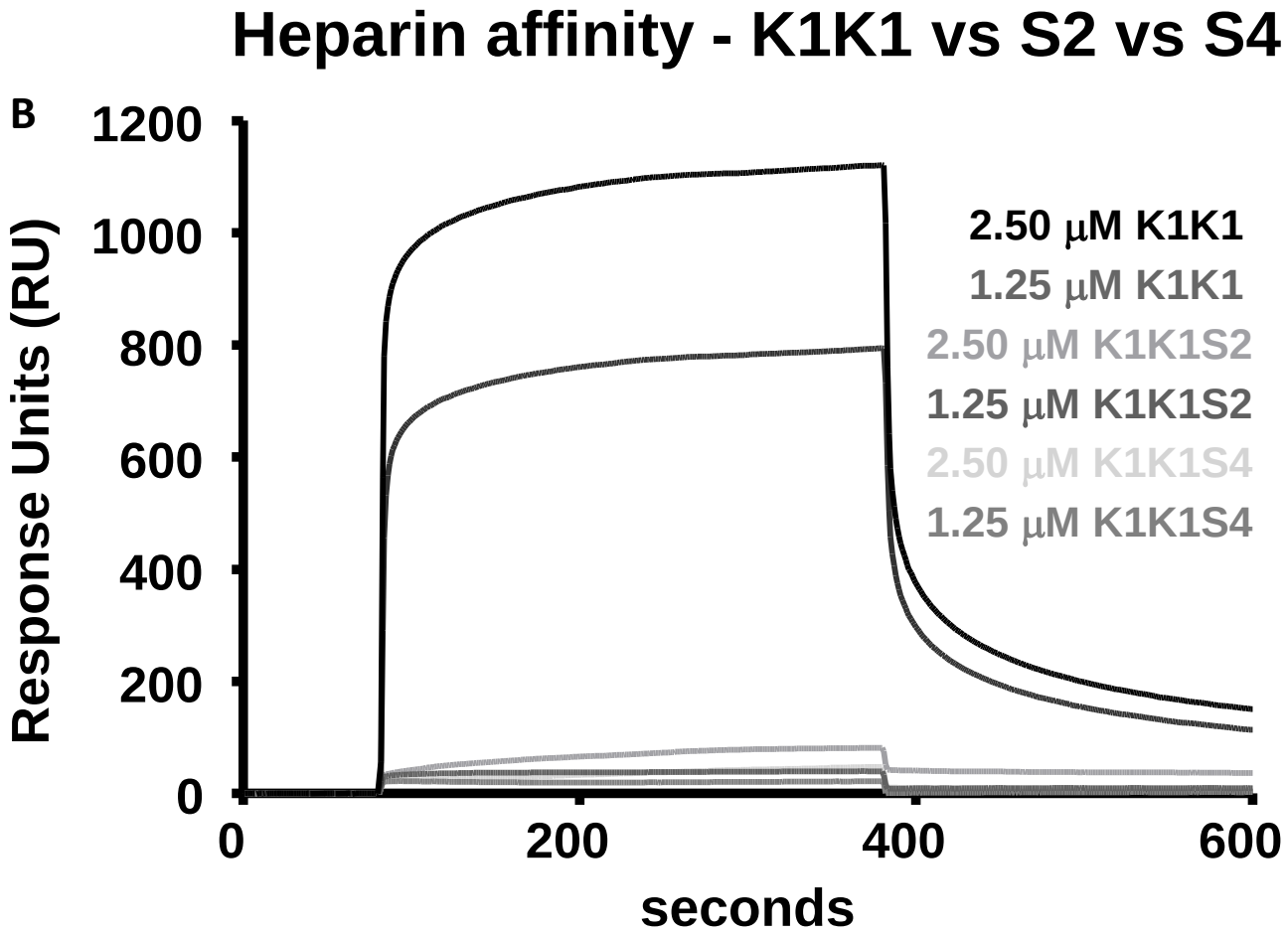

Images Data Source File

Ctrl

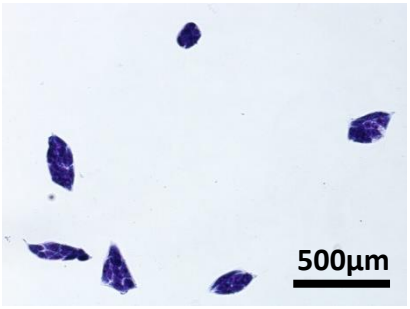

HGF/SF 300 pM

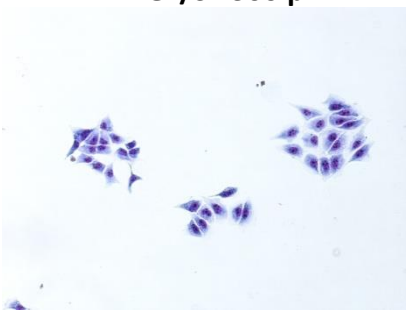

K1K1 100 nM

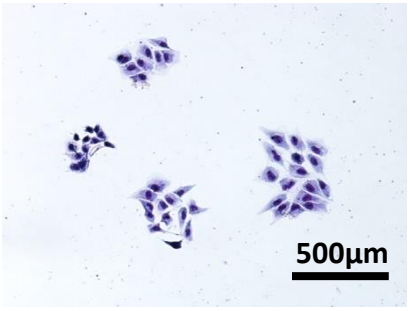

K1K1 30 nM

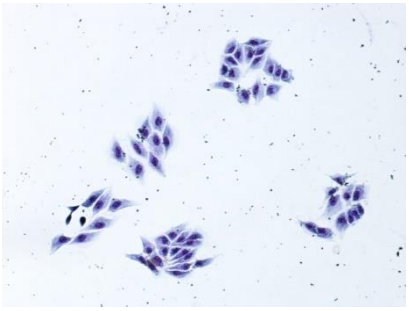

K1K1 10 nM

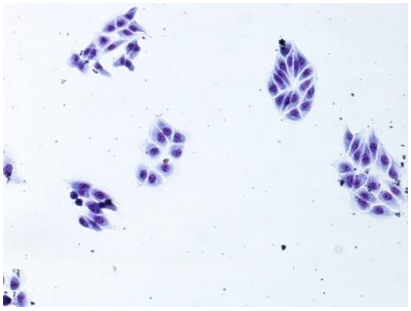

K1K1 3 nM

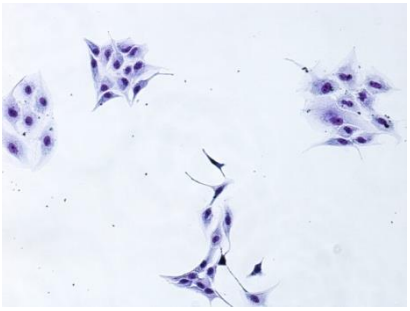

K1K1 1 nM

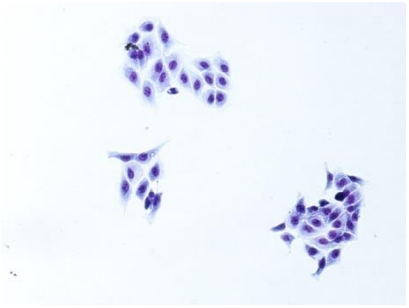

K1K1 300 pM

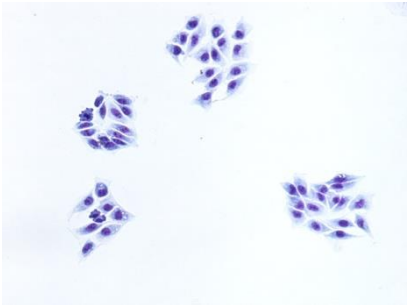

K1K1 100 pM

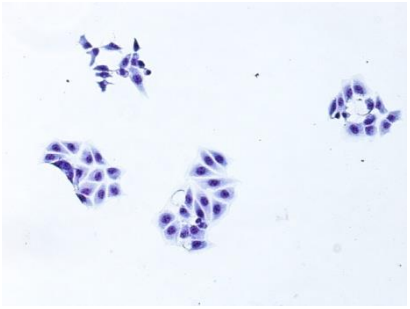

K1K1 30 pM

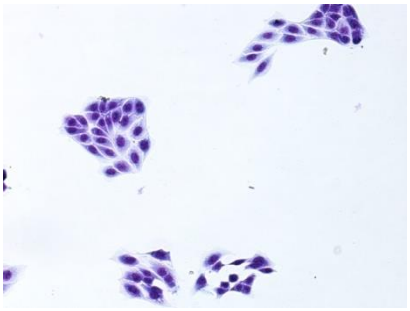

K1K1 10 pM

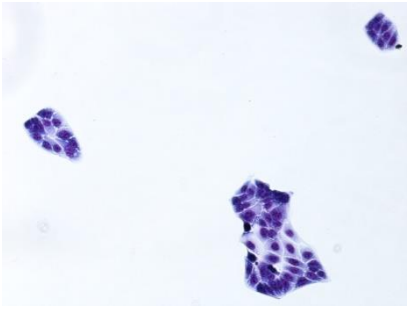

X40 Nikon Eclypse Bright Field

Images Data source Files

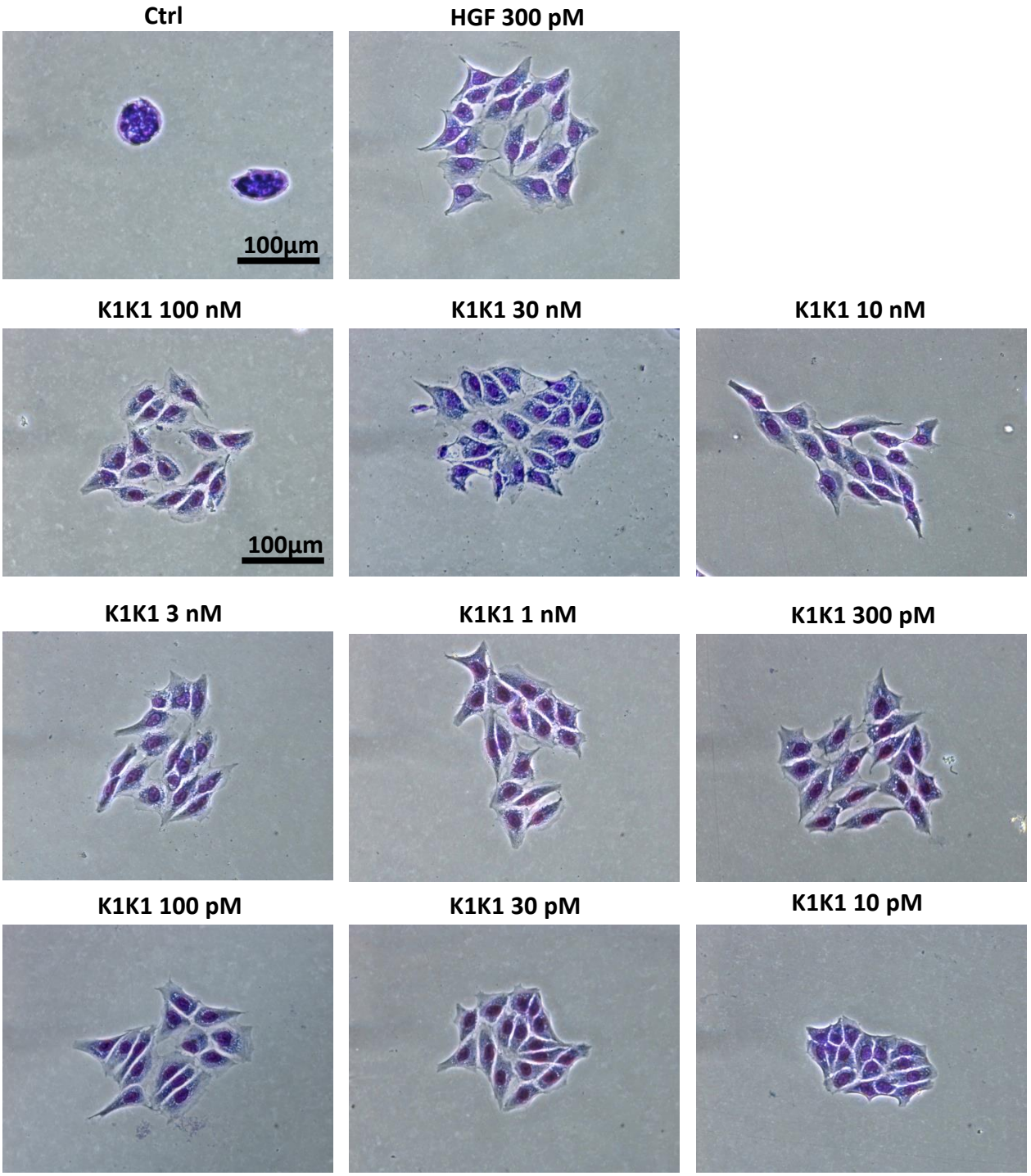

X200 Nikon Eclypse Bright Field

Data Source File

Supplementary figure 3

C

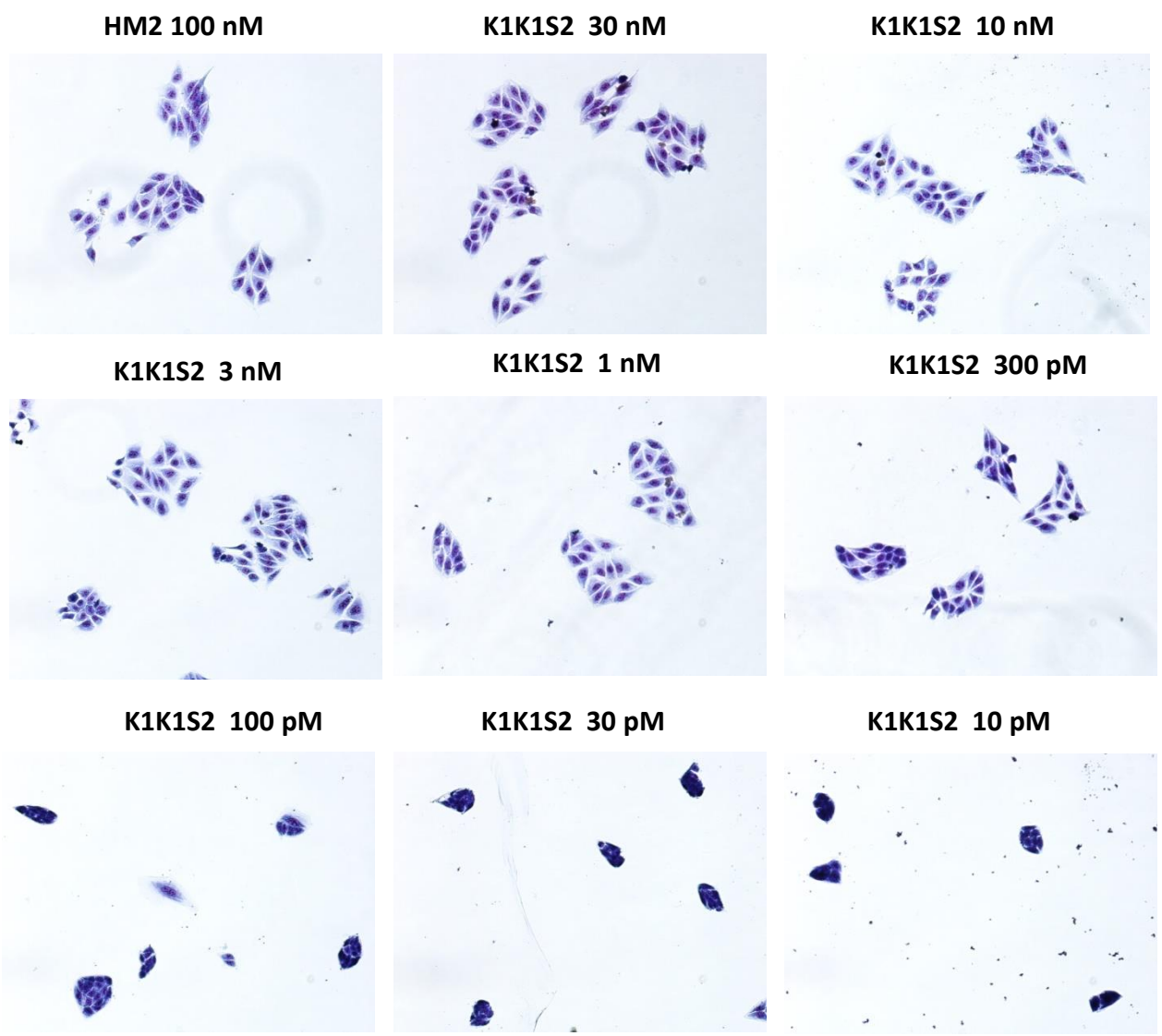

X40 Nikon Eclypse Bright Field

K1K1S2 100 nM

K1K1S2 30 nM

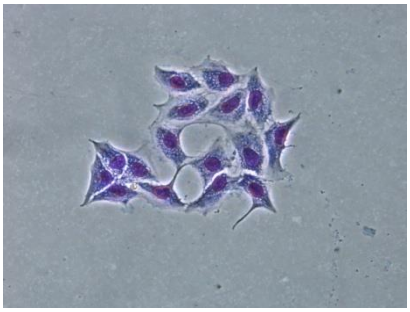

K1K1S2 10 nM

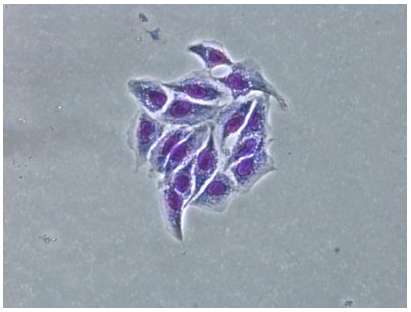

K1K1S2 3 nM

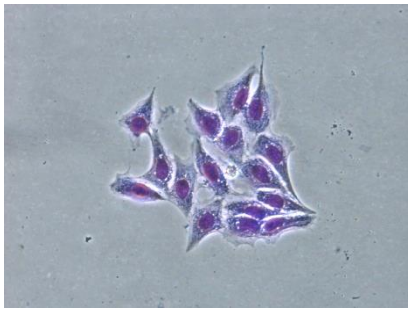

K1K1S2 1 nM

K1K1S2 300 pM

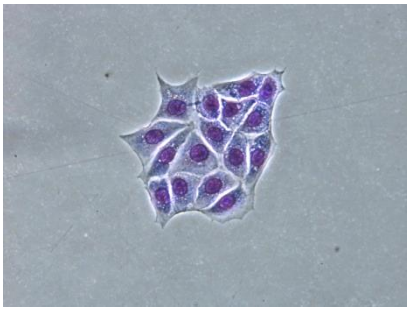

K1K1S2 100 pM

K1K1S2 30 pM

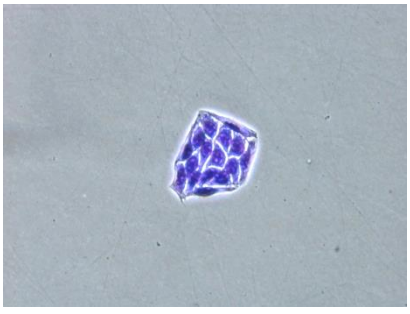

K1K1S2 10 pM

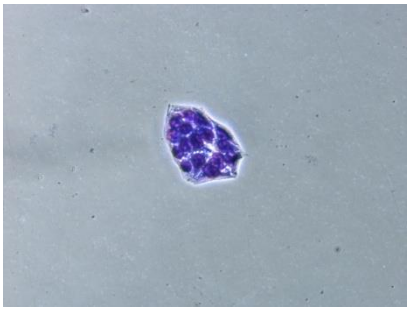

X200 Nikon Eclypse Bright Field

Data Source File

D

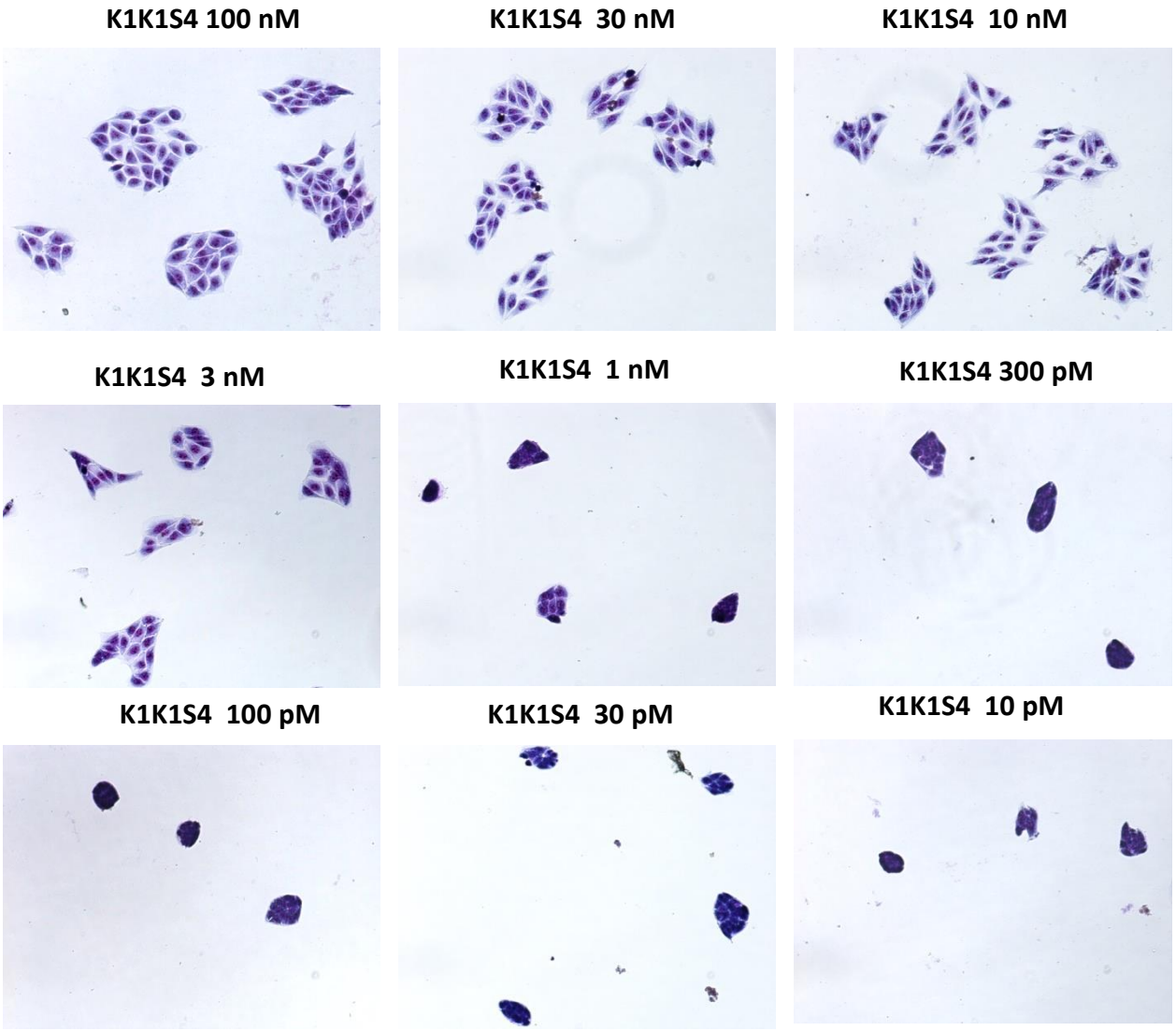

X40 Nikon Eclypse Bright Field

Data Source File

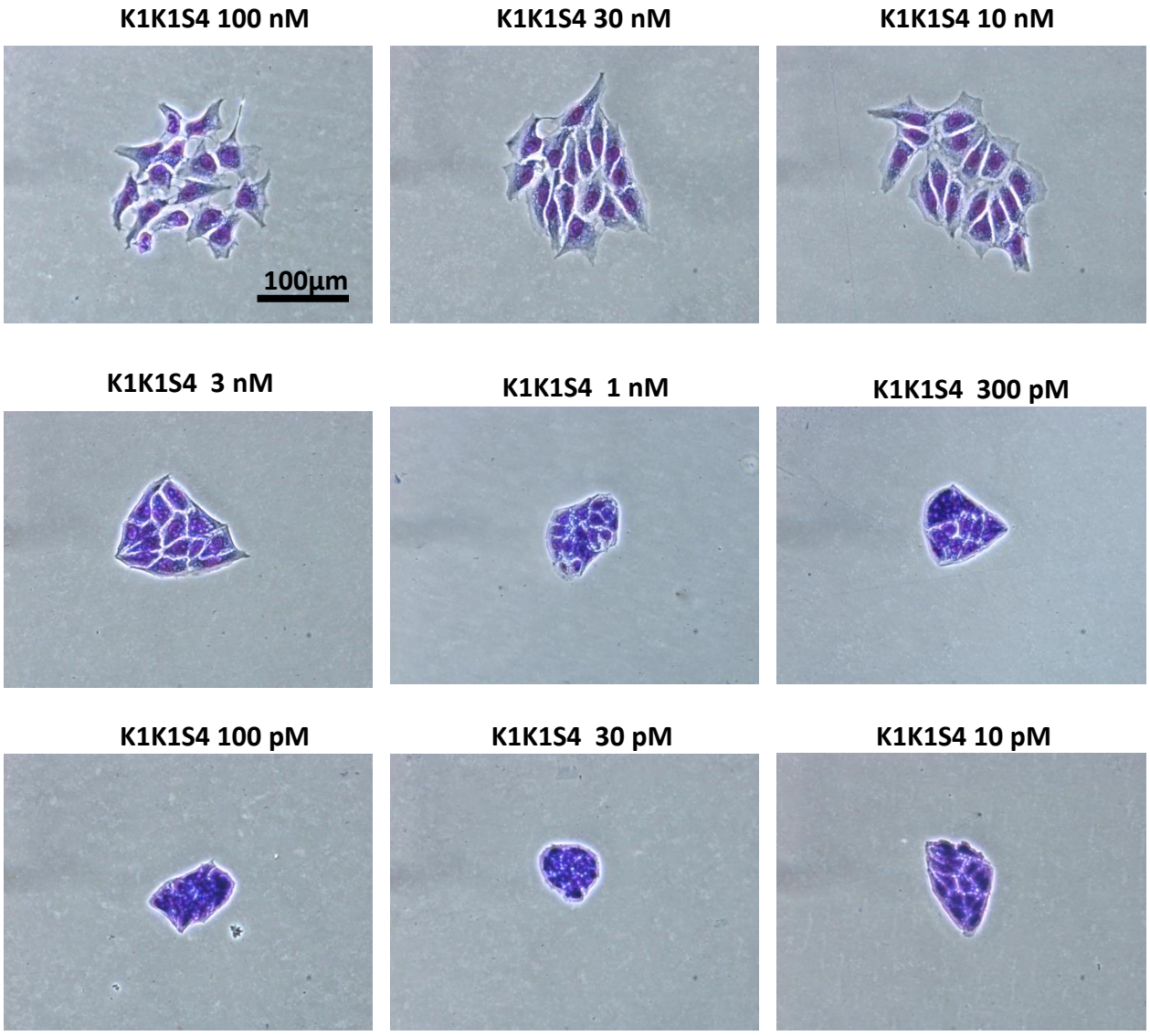

X200 Nikon Eclypse Bright Field